PHOTOCHEMICAL DISSOLUTION OF MICROPLASTICS IN SEAWATER

DISSOLUTION PHOTOCHIMIQUE DES MICROPLASTIQUES DANS L'EAU DE MER

Mémoire présenté

dans le cadre du programme de maîtrise en océanographie

en vue de l'obtention du grade de maître ès sciences

par

© **Mengyue Wu**

Août 2021

Composition du jury :

Dr. Zhe Lu, président du jury, UQAR-ISMER, Rimouski, Canada

Dr. Sophia Johannessen, examinatrice externe, IOS, Sidney, Canada

Dr. Huixiang Xie, directeur de recherche, UQAR-ISMER, Rimouski, Canada

Dr. Rong Ji, codirecteur de recherche, NJU, Nanjing, China

Dépôt initial le 26 Avril 2021 Dépôt final le 03 Août 2021

REMERCIEMENTS

Je tiens à exprimer ma plus profonde gratitude à mon directeur, Huixiang Xie, pour toutes ses idées constructives et la révision rigoureuse de mon mémoire, pour sa patience et ses encouragements tout au long de ce projet. Je tiens à remercier mon co-directeur, Rongji, d'avoir fourni du matériel d'expérimentation pour ce projet, pour son aide dans l'analyse des données et ses commentaires constructifs sur ce mémoire.

Je tiens également à remercier Claude Belzile pour son aide dans le traitement des données sur le DOC et sur l'abondance des bactéries, Jean-François Hélie et Mathieu Babin pour avoir analysé la composition élémentaire des microplastiques, Yijie Li et Amélie Évrard pour leur aide dans la collecte d'échantillons et pour m'avoir guidée dans l'utilisation des instruments. Un grand merci à Loïc Mas d'avoir corrigé la traduction du résumé en français. Je remercie aussi tous mes professeurs et mes amis de l'ISMER qui m'ont encouragée et soutenue pendant mon projet.

Cette recherche a été financée par le Conseil de recherches en sciences naturelles et en génie du Canada (CRSNG). J'ai été soutenue par les bourses du CRSNG et de l'Institut des sciences de la mer de Rimouski.

ACKNOWLEDGMENTS

I would like to express my deepest gratitude to my supervisor, Huixiang Xie, for his constructive ideas, rigorous review of this thesis, his patience and encouragement throughout this project. Many thanks are extended to my co-supervisor, Rong Ji, for providing the microplastic samples to this project, his help with data analysis, and his constructive comments on this thesis.

I would also like to thank Claude Belzile for the analysis of dissolved organic carbon and bacteria abundance, Jean-François Hélie and Mathieu Babin for the analysis of the elemental composition of microplastics, Yijie Li and Amélie Évrard for their help in collecting samples and in the use of the instruments related to this project, and Loic Mas for correcting the translation of the abstract into French. I also thank all my teachers and friends at the Institut des sciences de la mer de Rimouski (ISMER) who encouraged and supported me during my study.

This research was funded by the Natural Sciences and Engineering Research Council of Canada (NSERC). I was supported by grants from NSERC and the Institut des sciences de la mer de Rimouski.

RÉSUMÉ

Les plastiques présents dans l'océan y sont très largement répandus, et créent quantité d'effets néfastes pour les écosystèmes marins comme pour les êtres humains. Parmi cette pollution, les microplastiques (abrégés en « MPs », <5 mm en diamètre) sont le type de plastique le plus abondant dans l'océan, lorsqu'on compte en nombre de particules. Ils sont à l'origine de vives inquiétudes environnementales et sociétales contemporaines, car leur taille microscopique leur permet d'être ingérés par d'autres organismes, bioaccumulés dans la chaîne alimentaire et transportés sur de grandes distances et pendant de longues périodes. Ainsi, comprendre la transformation et l'avenir des microplastiques est crucial pour mieux estimer leurs impacts environnementaux, puis y répondre. Bien que la photooxydation ait été envisagée comme le processus de dégradation le plus efficace des plastiques à la surface de l'océan, les connaissances quantitatives de ce processus restent limitées, en particulier pour les MPs de petite taille. Notre étude cherche en partie à répondre à ce problème, car elle vise à fournir de nouvelles données pertinentes pour évaluer comment la conversion photochimique des MPs en matière organique dissoute (c'est-à-dire la photodissolution) va affecter leur avenir à la surface des mers et des océans. Pour cela, des MPs d'une taille inférieure au millimètre et de trois types très répandus (polypropylène (PP), polystyrène (PS), uréthanne thermoplastique (TPU) ont été incorporés à de l'eau de mer artificielle et irradiés dans un simulateur solaire. Les taux de photodissolution des MPs ont été déterminés en termes de photoproduction de carbone organique dissous (DOC), de matière organique dissoute chromophorique (CDOM, représentée par le coefficient d'absorption à 254 nm), et d'azote dissous (DN) dans le cas du TPU. Les effets de la température de l'eau et de la composition de la lumière incidente sur la photodissolution des MPs ont aussi été évalués. Sous irradiation à spectre complet, les photoproductions de DOC et de CDOM ont été observées pour chacun des trois types de microplastiques, ainsi qu'une libération de DN

pour le TPU ; leurs taux de production ayant augmenté exponentiellement sur une période d'irradiation de 7 jours. Le TPU et le PS étaient plus photodégradables que le PP, d'après le pourcentage de photodissolution du carbone plastique. Le CDOM photoproduit à partir du PP présentait un pic d'absorption à 292 nm caractéristique des cétones aliphatiques. La dépendance de la photodissolution à la température a augmenté avec le temps d'irradiation pour ce qui est du PP et du PS. En revanche, elle est restée plutôt constante pour le TPU. Pour une augmentation de 20°C de la température, le taux de photoproduction de DOC a augmenté de 970% pour le PP, de 288% pour le PS et de 413% pour le TPU à la fin d'une irradiation de 7 jours, avec une énergie d'activation comprise entre 59,4 et 84,8 kJ mol^{-1}. La photodissolution des MPs était presque exclusivement induite par le rayonnement ultraviolet-B (UVB : 290–320 nm), avec assez peu d'effets pour les UVA (320–400 nm) et le rayonnement visible. La DOM photoproduite depuis le PS était au moins en partie photominéralisable, tandis que la DOM photoproduite à partir du PP et du TPU a semblé résistante à la photominéralisation. L'extrapolation des taux de photoproduction du DOC obtenus en laboratoire à l'océan de surface donne des estimations de durées de vie de 6,5 ans pour le PP, de 3,6 ans pour le PS et de 3,7 ans pour le TPU dans les eaux chaudes. Cela suggère que la photodissolution peut être un mécanisme important pour expliquer l'absence de puits de plastiques de taille inférieure à un millimètre observée dans les gyres subtropicaux de l'Atlantique Nord et du Pacifique Nord. Les résultats de cette étude indiquent également que la variation de température de l'eau semble un facteur plus important que le changement de l'irradiation pour déterminer les taux de photodissolution des MPs, lorsqu'ils passent des eaux chaudes aux eaux froides ou vice versa.

Mots-clés : Microplastiques, photodégradation, eau de mer, carbone organique dissous, matière organique dissoute chromophorique, azote dissous

ABSTRACT

Plastics in the ocean are widespread and pose adverse effects to marine ecosystems and human beings. Microplastics (MPs, <5 mm in diameter) are the most abundant plastic form in the ocean in terms of number of pieces. MPs draw particular environmental and societal concerns because their small sizes allow them to be ingested by organisms, bioaccumulated in the food web, and transported over larger time and space scales. Understanding the transformation and fate of MPs is thus crucial for assessing their environmental impacts. Although photooxidation has been proposed as the most efficient degradation process of plastics in the surface ocean, quantitative knowledge of this process remains limited, particularly for smaller-sized MPs. This study aims to provide new data that are useful for assessing the role of photochemical conversion of MPs to dissolved organic matter (i.e. photodissolution) in controlling the fate of MPs in the surface ocean. Three common types of MPs with sub-millimeter sizes polypropylene (PP), polystyrene (PS), and thermoplastic polyurethane (TPU) were irradiated in artificial seawater under solar-simulated radiation. The photodissolution rates of the MPs were determined in terms of photoproduction of dissolved organic carbon (DOC), chromophoric dissolved organic matter (CDOM, represented by the absorption coefficient at 254 nm), and dissolved nitrogen (DN) as well, in the case of TPU. The effects of water temperature and incident light composition on the photodissolution of MPs were evaluated. Under full-spectrum irradiation, the photoproduction of DOC and CDOM was observed in all three microplastic samples and DN in TPU; their production rates increased exponentially over an irradiation period of 7 days. TPU and PS were more photodegradable than PP based on the percent plastic carbon photodissolution. CDOM photoproduced from PP exhibited an absorption peak at 292 nm, which is characteristic of aliphatic ketones. The temperature dependence of photodissolution increased with irradiation time for PP and PS but remained essentially constant for TPU. For a 20°C

increase in temperature, the photoproduction rate of DOC increased by 970% for PP, 288% for PS, and 413% for TPU at the end of a 7-d irradiation, with the activation energy in the range of 59.4–84.8 kJ mol^{-1}. Photodissolution of the MPs was almost exclusively driven by ultraviolet-B (UVB: 290–320 nm) radiation, with little impact by UVA (320–400 nm) and visible radiation. DOM photoproduced from PS was at least partially photomineralizable, while DOM photoproduced from PP and TPU appeared resistant to photomineralization. Extrapolation of the lab-based DOC photoproduction rates to the surface ocean yields lifetime estimates of 6.5 years for PP, 3.6 years for PS, and 3.7 years for TPU in warm waters, suggesting that photodissolution can be a significant mechanism for explaining the missing sink of sub-millimeter-sized plastics in the subtropical gyres in the North Atlantic and the North Pacific. The results from this study also indicate that the change in water temperature is more important than the change in irradiance in controlling the photodissolution rates of the MPs when they move from warm waters to cold waters or vice versa.

Keywords: Microplastics, photodegradation, seawater, dissolved organic carbon, chromophoric dissolved organic matter, dissolved nitrogen

TABLE OF CONTENTS

LIST OF TABLES

LIST OF FIGURES

LIST OF ABBREVIATIONS

Abbreviations	Signification	
	Français	**Anglais**
ASW	Eau de mer artificielle	Artificial seawater
CDOM	Matière Organique Dissoute Chromophorique	Chromophoric dissolved organic matter
DIN	Azote inorganique dissous	Dissolved inorganic nitrogen
DN	Azote dissous	Dissolved nitrogen
DOC	Carbone organique dissous	Dissolved organic carbon
DOM	Matière Organique Dissoute	Dissolved organic matter
DON	Azote organique dissous	Dissolved organic nitrogen
HDPE	Polyéthylène haute densité	High-density polyethylene
LDPE	Polyéthylène basse densité	Low-density polyethylene
LLDPE	Polyéthylène basse densité linéaire	Linear low-density polyethylene
MPs	Microplastiques	Microplastics
t	Tonnes métriques	Metric tonnes
PE	Polyéthylène	Polyethylene
PET	Polytéréphtalate d'éthylène	Polyethylene terephthalate
PC	Polycarbonate	Polycarbonate
POM	Matière organique particulaire	Particulate organic matter
PP	Polypropylène	Polypropylene
PS	Polystyrène	Polystyrene
PUR	Polyuréthane	Polyurethane
PVC	Polychlorure de vinyle	Polyvinyl chloride
ROS	Espèces réactives de l'oxygène	Reactive oxygen species
TPU	Polyuréthane thermoplastique	Thermoplastic polyurethane
UV	Ultraviolet (280–400 nm)	
UVA	Ultraviolet-A (320–400 nm)	
UVB	Ultraviolet-B (280–320 nm)	
UVC	Ultraviolet-C (200–280 nm)	

LIST OF SYMBOLS

Symbols	Definition	Units
$A(\lambda)$	Absorbance at wavelength λ	Dimensionless
$a_{CDOM}(\lambda)$	CDOM absorption coefficient at wavelength λ nm	m^{-1}
$a_{CDOM}(254)$ (a_{254})	CDOM absorption coefficient at wavelength 254 nm	m^{-1}
C_0	Initial carbon content in microplastics	µmol
C/N	Molar ratio of carbon to nitrogen	Dimensionless
C/O	Molar ratio of carbon to oxygen	Dimensionless
[DN]	Concentration of dissolved nitrogen	µmol L^{-1}
[DOC]	Concentration of dissolved organic carbon	µmol L^{-1}
E_a	Activation energy	J mol^{-1}
P_{CDOM}	Photoproduction rate of chromophoric dissolved organic matter	m^{-1} d^{-1}
P_{DN}	Photoproduction rate of dissolved nitrogen	µmol L^{-1} d^{-1}
P_{DOC}	Photoproduction rate of dissolved organic carbon	µmol L^{-1} d^{-1}
$SUVA_{254}$	Specific UV absorption coefficient (decadic, i.e. base 10) at 254 nm	L mg^{-1} m^{-1}
T	Temperature	K or °C
R	Universal gas constant	8.314 J K^{-1} mol^{-1}
UVB_{lab}	Integrated UVB (280–320 nm) irradiance of the solar simulator	mmol cm^{-2} d^{-1}
UVB_{sea}	Integrated UVB (280–320 nm) irradiance just above the sea surface	mmol cm^{-2} d^{-1}
µmol	Micromoles	
λ	Wavelength	nm
V	Initial volume of the microplastic suspension sample in the irradiation cell	L
τ_{sea}	The lifetime of a given type of microplastics with respect to photodissolution at the sea surface	years

1. INTRODUCTION

1.1. PLASTIC POLLUTION IN THE OCEANS

Since the beginning of the mass production of plastics in the 1940s, the global plastic production has increased tremendously, from 1.5 million metric tonnes (t) in 1950 to 368 million t in 2019 (Plastics Europe, 2020). Commonly-used plastics include polypropylene (PP, 21.0%), low-density and linear low-density polyethylene (LDPE and LLDPE, 20.0%), high-density polyethylene (HDPE, 16.3%), and polyvinyl chloride (PVC, 11.8%). Other types of plastics with significant presence are polyethylene terephthalate (PET, 10.2%), polyurethane (PUR, 8.2%) and polystyrene (PS, 7.6%) (Figure 1) (Geyer et al., 2017). Despite the continuously-growing production, the recycling of plastics has been managed poorly, leading to the accumulation of plastics in the environment. Cumulative plastics waste amounted to 6.3 billion t from 1950 to 2015. Only 600 million t (9%) of plastics were recycled effectively, while ~4900 million t (60%) of all plastics ever produced have ended up in landfills and natural environments (Geyer et al., 2017).

The first scientific reports of plastic pollution in the oceans emerged in the early 1970s (Bascom, 1974; Colton et al., 1974). In the recent decades plastic pollution has caused sustained concerns in the scientific community. Owing to its widespread use, lightweight, buoyancy, and durability, plastics are extensively distributed in the world′s oceans. According to a modeling study by Eriksen et al. (2014), five trillion plastic particles are afloat in the world's oceans, with a total weight of over 250,000 t. Jambeck et al. (2015) estimated that 4.8 to 12.7 million t of plastics entered the ocean from 192 coastal countries in 2010. Following this prediction, the cumulative quantity of land-

derived plastics in the ocean is expected to increase by an order of magnitude by 2025 if world plastics consumption continues without an improvement in waste management.

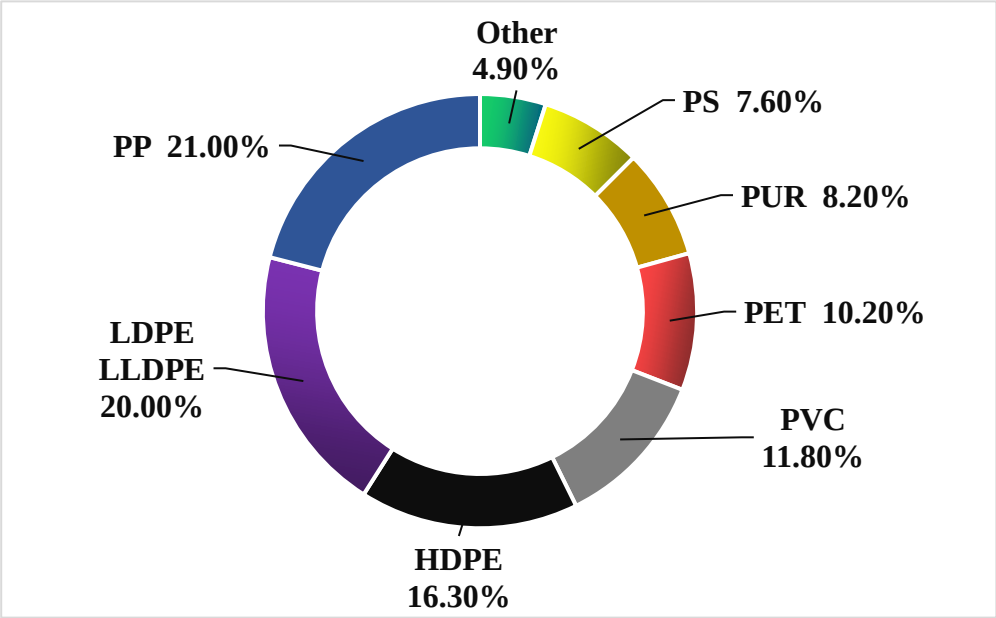

Figure 1: Share of total polymer resin production according to polymer type, calculated from data for Europe, the United States, China, and India, covering the period 2002–2014. LLDPE = Linear Low Density Polyethylene; LDPE = Low Density Polyethylene; HDPE = High Density Polyethylene; PP = Polypropylene; PS = Polystyrene; PVC = Polyvinyl Chloride; PET = Polyethylene Terephthalate; PUR = Polyurethane. Note that the above table is for non-fibers only; polyester, polyamide, and acrylic fibers are not included. (Source: Geyer et al., 2017)

1.2. MICROPLASTICS IN THE MARINE ENVIRONMENT

Microplastics (MPs) are a heterogeneous group of plastics particles ranging in size from a few micrometers to several millimeters in diameter (Thompson et., 2004). Arthur et al. (2009) broadened the definition of MPs to all plastic fragments with a size below 5

mm. Thompson et at. (2004) first reported microscopic plastic fragments in marine sediments and in the water column of Plymouth, UK. They also found that marine organisms such as amphipods, lugworms and barnacles ingested MPs within a few days of laboratory trials. In recent years, MPs have created major environmental and societal concerns and numerous articles on their sources, occurrences, fates, and ecological effects have been published. Scientific interest on this topic will continue, since plastic pollution remains a major environmental problem (Andrady, 2011; Cole et al., 2011; Law and Thompson, 2014; Auta et al., 2017; Alimba et Faggio, 2019).

1.2.1. Sources

MPs are usually generated from two sources: primary MPs and secondary MPs. Primary MPs are the plastics that are manufactured to be of microscopic size, such as microbeads in certain personal care products, industrial abrasive scrubbers, microfibers in synthetic textiles, and virgin plastic pellets used as raw materials for plastic production (Andrady, 2011). About 1.5 million tons of primary MPs are released into the world´s oceans annually, accounting for 15–30% of all the plastic pollution in the oceans (Boucher and Friot, 2017). About 96.3% of these primary microplastics are from land-based sources, with the rest from marine coating.

Secondary MPs are generated from the abrasion and fragmentation of larger plastic debris in the environment by physical, chemical, and biological processes, such as wave action, turbulence, ultraviolet (UV) radiation, and bacterial degradation (Andrady, 2011; Cole et al., 2011). The rates of plastic weathering in beach, surface-water, and deep-water environments are very different. Low-oxygen, dark, and cold conditions limit plastic weathering. Beaches are the most common sites for the generation of secondary microplastics in the marine environment through *in situ* weathering of plastic litter. Plastics on beaches degrade rapidly under exposure to high oxygen concentrations and high temperatures (up to ~40°C on sandy beaches). After the destruction of the structural integrity and formation of cracks on the surface, plastics can be more easily fragmented to MPs by abrasion, wave action, and turbulence (Andrady, 2011).

Plastic litter with a terrestrial source contributes ~80% of the plastic debris in the marine environment (Andrady, 2011). With large amounts of big plastic items present and continuing to accumulate in the environment, the abrasion and fragmentation of macroplastics is probably the most relevant source of MPs in the marine environment (Duis and Coors, 2016).

1.2.2. MPs accumulation in surface oceans

MPs are ubiquitous in the marine environment, from coastal seas to open oceans and from equatorial areas to polar regions. It has been estimated that MPs account for 92.4% of the global plastic particle count and that over 4.85 trillion microplastic particles, together weighing 35,540 t, are floating in the world′s oceans (Eriksen et al., 2014). The distribution of MPs in the marine environment is uneven and largely depends on the densities of the particles, ocean hydrodynamics, and environmental factors. Plastic density plays a key role in controlling plastics distributions in the water column. Low-density plastics float in surface water, driven by wind and surface circulation, while plastics heavier than seawater sink to the seafloor. Processes such as ingestion by organisms, biofilm formation, aggregation, incorporation into marine snow, and vertical transport caused by wind mixing may remove buoyant MPs from surface water (Hale et al., 2020).

Many investigations were carried out during the last decade to estimate the loads of MPs in the Pacific Ocean, the Atlantic Ocean, Asian seas, the Mediterranean Sea, the Antarctic, and Arctic Oceans. A literature review of MP concentrations in global surface oceans is shown in Table S1. Average concentrations in coastal seas range from 0.15 (de Lucia et al., 2014) to 16,272 particles m^{-3} (Zhao et al., 2014), with a median value of 27.2 ± 52.5 particles m^{-3}. The highest concentration has been found in East China Sea and lowest in Sardinian Sea. The median concentration in coastal seas is over 16 times higher than that in open oceans (see below). The much higher concentration in coastal seas is due to their proximity to the land, which is the dominant source of MPs to the ocean. Transport of MPs from the land to coastal seas is mainly through river discharges

and sewage discharge (e.g. Zhao et al., 2014; Cózar et al., 2015; Tsang et al., 2017; Zhu at al., 2018). Storm water runoff, industrial activities, and losses from accidental spilling and transport are also major sources of plastic pollution in coastal regions (Tsang et al., 2017). Notably, concentrations of up to 66,666 particles m^{-3} and 359,748 particles m^{-3} of MPs were reported in the sea surface microlayer of Geoje Island (Song et al., 2014) and the Incheon/Kyeonggi Coastal Region (Chae et al., 2015), respectively due in part to the inclusion of smaller-sized MPs and certain nanoplastics (down to 0.75 μm).

In the open ocean, MP concentrations range from 0.006 (Pan et al., 2019) to 457 particles m^{-3} (Desforges et al., 2014), with a median value of 1.69 particles m^{-3}. The most extensive MPs accumulations are found in five major ocean gyres: The North and South Pacific Subtropical Gyres, the North and South Atlantic Subtropical Gyres, and the Indian Subtropical Ocean Gyre (Moore et al., 2001; Lavender Law et al., 2010; Goldstein et al., 2013; Eriksen et al., 2013; Desforges et al., 2014; Law et al., 2014; Lusher et al., 2014; Lebreton et al., 2018). Floating plastics accumulate in these gyres, due to rotating ocean currents and form "garbage patches". The observation of the accumulation of MPs in the subtropical gyres is consistent with the modeling results of Eriksen et al. (2014) (Figure 2).

Notably, despite an increasing input of plastics to the ocean during the last several decades, no long-term trends have been observed in the concentration of plastics afloat in the subtropical ocean gyres, implying the existence of processes that can rapidly remove plastics from the surface ocean (Lavender Law et al., 2010; Law et al. 2014). In particular, the measured concentrations of MPs are far below those expected from modeling studies (Cózar et al., 2014; Eriksen et al., 2014). The exact mechanisms for this source-sink imbalance (i.e. missing sink) are unclear but have been attributed to photo- and bio-fragmentation of MPs to nanoplastics (<100 nm in size), ingestion by organisms, decreased buoyancy due to fouling organisms and association with marine snow, shore deposition by waves or other undiscovered processes (Cózar et al., 2014; Eriksen et al., 2014).

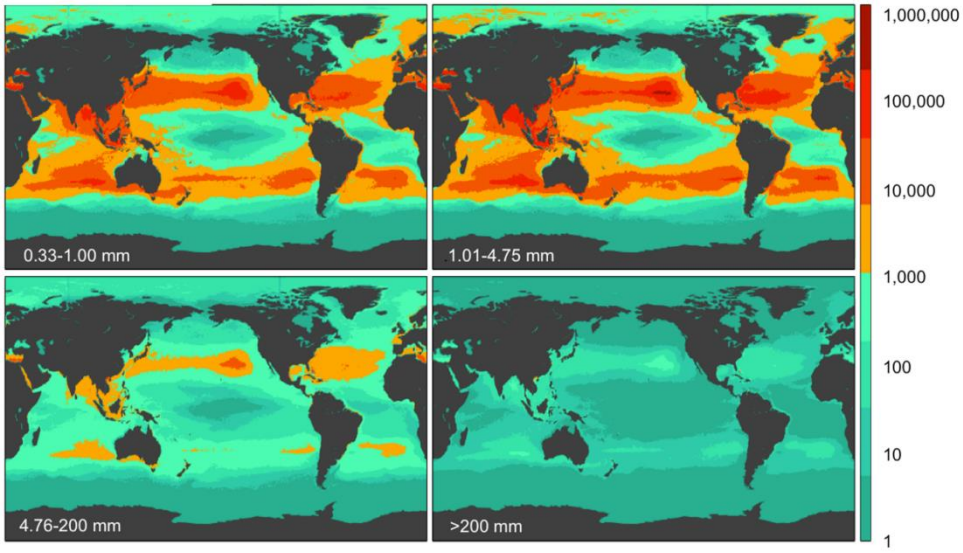

Figure 2: Model results for global count density in four size classes of plastics. Units: pieces km^{-2}. (Source: Eriksen et al., 2014).

1.2.3. Impacts of MPs in marine environment

MPs in the ocean have created major environmental and societal concerns during the last several decades as these pollutants are widespread in every corn of the oceans, and are available to marine organisms. Once ingested by the organisms, the potential adverse effects on the organisms are not only from the ingested MPs themselves but could also result from the leaching of inherent additives from MPs, and from the disassociation of the pollutants adhered to the MPs from surrounding environment (Cole et al., 2011; Van Cauwenberghe, 2016).

MPs are ingested by a wide range of marine organisms, both in natural environments and in laboratory exposures, including seabirds (Provencher et al., 2018), turtles (Caron et al., 2018), zooplankton (Desforges et al., 2015), fishes (Neves et al., 2015), benthos (Wright et al., 2013a), and marine mammals (Nelms et al., 2018). As MPs have similar sizes and densities to those of microplankton, many marine organisms, especially

planktonic species, cannot distinguish MPs from food and prey. Once ingested by organisms, microplastics may excrete out of their bodies or accumulate in their tissues. After being taken up by zooplankton, MPs can be transferred to higher trophic levels, which poses a potential risk to higher trophic level species (Farrell and Nelson, 2013; Setälä et al., 2014; Nelms et al., 2018). The accumulation of MPs in tissues may cause several potential threats to marine organisms, including false satiation and physiological stress from the blockage of the gut tract (Wright et al., 2013b), reduction in feeding capacity and mobility (Watts et al., 2014; Lönnstedt and Eklöv, 2016), slow growth (Watts et al., 2014), low reproduction (Lee et al., 2013; Sussarellu et al., 2016), and increased mortality (Au et al., 2015; Rist et al., 2016).

Many additives, including plasticizers, flame retardants, antioxidants and heat stabilizers, are widely used in the manufacturing of plastics to make them durable, flexible, lightweight, water-, light- and fire-resistant (Hahladakis et al., 2018; Galloway et al., 2019). However, these additives may leach out to the environment and biota during the abrasion of plastics. Microplastics can adsorb many pollutants, including metals (e.g. Ag, Cd, Co, Ni, Pb and Zn) (Turner and Holmes, 2015) and persistent organic pollutants (e.g. polycyclic aromatic hydrocarbons, polychlorinated biphenyls, and dichloro-diphenyl-trichloroethanes) (Zhang et al., 2015), due to their large surface area to volume ratios and high hydrophobicity. MPs alone or in combination with hazardous substances can be transported across oceans and pollute pristine ecosystems, or be transferred through the food web following ingestion by marine organisms (Talsness et al., 2009; Browne et al., 2013 Rochman et al., 2014).

There is evidence that MPs may have entered the human body through food, especially seafood (Yang et al., 2015; Van Cauwenberghe and Janssen, 2014; Pivokonsky et al., 2018), thereby causing potential risks for human health. For instance, the alternate ingestion of microparticles can cause alteration in chromosomes, which leads to infertility, obesity and/or cancer (Sharma and Chatterjee, 2017).

1.3. NON-PHOTOCHEMICAL DEGRADATION OF PLASTICS IN THE MARINE ENVIRONMENT

Plastic degradation refers to the processes that change plastic properties under the influences of physical, chemical, or biological reactions that result in bond scission and subsequent chemical transformations (Pospíšil and Nešpůrek, 1997). Degradation leads to changes in material properties, such as tensile strength, color, shape, and molecular weight, durability, etc., under the influence of one or more environmental factors, such as heat, light or exposure to chemicals (Jasso-Gastinel et al., 2017). Furthermore, the plastics can be completely mineralized to CO_2 via microbial-mediated biodegradation or photochemical degradation (Andrady, 2011; Klein et al., 2018; Ward et al., 2019; Tian et al., 2019). The degradation of plastics in the marine environment is slow compared to terrestrial exposure (Kershaw et al., 2011) and is effected by four major pathways: hydrolytic, thermal oxidative, photochemical, and biological degradation (Andrady, 2011).

Hydrolysis of polymers is defined as the cleavage of polymer chemical bonds by the reactions with water molecules (Padsalgikar, 2017). This reaction mainly occurs in the polymers that easily absorb moisture into their surfaces and that have water-sensitive groups in their backbone (Polymer Properties Database, 2015). The carbonyl group, composed of a carbon double-bonded to an oxygen (C=O), is the most susceptible to hydrolysis. The carbonyl bond could be attached to oxygen, nitrogen or other atoms, and these bonds could be anhydrides, esters, amides, carbonates, or urethanes. The relatively high pH of seawater (8–8.3) suggests that hydrolysis may be important in this environment (Min et al., 2020).

Thermal oxidative degradation, a slow oxidative breakdown at moderate temperatures, is one of the environmental degradation mechanisms that are affected by temperature and oxygen (Andrady, 2011). In order for plastics to undergo thermal oxidative degradation, a sufficient input of energy in the form of heat is essential in order to break chemical bonds and initiate reactions. This process creates a highly reactive and

unstable polymer ‘free radical’ (R*) and a hydrogen atom with an unpaired electron (H*). Then, these radicals react with oxygen to form peroxide radicals (ROO*), which subsequently decompose further to form highly reactive hydroxyl free radicals (*OH) and alkoxy radicals (RO*). The formation of these reactive radicals will continue to react with oxygen or other polymers, thereby propagating the chain reaction. The reaction will continue to self-propagate until the energy input or oxygen supply is terminated. The reaction can also be terminated by radical recombination to form inert products (Figure 3) (Crawford and Quinn, 2016).

Biodegradation is the process by which the organic substances are broken down by living organisms, especially microorganisms such as bacteria and fungi. The biodegradation of plastics can occur both in aerobic and anaerobic environments. Plastics can be partially or completely converted to CO_2 (mineralization), H_2O, N_2, H_2, CH_4, salts, minerals or biomass (Klein et al., 2018). Generally, biodegradation follows after abiotic degradation, and its degradation rate is slower than those of other pathways (Andrady, 2015). Most synthetic plastics, such as PE, PP, PS, and PET, degrade very slowly or not at all, as they are water-insoluble. A combination of abiotic and biotic degradation pathways is needed for these plastics (Shah et al., 2008; Klein et al., 2018). In recent decades, biodegradable plastics have been developed to reduce plastic pollution in the environment (Rujnić-Sokele and Pilipović, 2017).

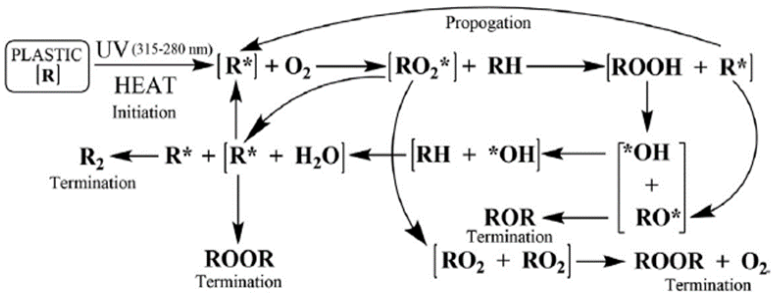

Figure 3: Polymer free radical chain reaction. (Source: Crawford and Quinn, 2016)

1.4. OVERVIEW OF AQUATIC ORGANIC MATTER PHOTOCHEMISTRY

A photochemical process is a chemical reaction that is initiated by light (Rohatgi-Mukherjee, 1978). Only light that is absorbed by chromophores can induce photochemical reactions (Grotthuss-Draper law) (Rohatgi-Mukherjee, 1978). Sunlight is the energy supply for photochemical reactions in aquatic environments. Since the ocean occupies 70% of the earth′s surface, most of the solar radiation that penetrates the atmosphere reaches the ocean. Averaged over the world′s oceans, 10–20% of incident solar radiation gets lost by scattering from the sea surface, leaving 80–90 % of the visible and UV radiation available to be absorbed by various chromophores (Zika, 1981). However, not all light absorbed by chromophores leads to photochemical reactions, since most of the absorbed light is utilized in photophysical processes (e.g. fluorescing, phosphorescing or energy transfer).

Chromophores in the ocean include dissolved inorganic and organic matter, suspended inorganic and organic particulate matter (living and dead) (Zika, 1981). In coastal and inland waters, light attenuation is mostly attributed to the dissolved substances and suspended particles. These materials can absorb solar radiation and limit light penetration to great depths, leading to shallow photic zones in coastal seas.

Photochemical reactions can be classified into two categories: direct photolysis and indirect photoreactions. Direct photolysis requires the presence of light-absorbing moieties (i.e. chromophoric groups) in the reactant itself to absorb light and then undergo photochemical reaction to form a product (Pelizzetti and Calza, 2002; Schwarzenbach et al., 2005). Since most compounds in natural waters are highly transparent to solar irradiation, direct photoreactions of these compounds are either impossible or represent only a minor reaction pathway (Cooper and Herr, 1987). According to some studies, nitrite and nitrate are the only inorganic compounds that can undergo direct photoreactions in the surface oceans, with nitrite being more photoreactive than nitrate (Zafiriou and True, 1979a,b). However, many organic chromophores with complex structures do participate in direct photoreaction processes in natural waters. Consequently,

direct photolysis may be the major process for degrading certain chemical pollutants which exhibit strong light absorption at wavelengths greater than 290 nm, such as pesticides, polycyclic aromatic hydrocarbons, and bisphenol A (Katagi, 2018; Jacobs et al., 2008; Chen et al., 2006).

Indirect photoprocesses are common and important, since they can alter molecules that are transparent and thus resistant to direct photolysis. Indirect photoreactions do not require the reactants themselves to possess chromophores, but require a photosensitizer to initiate the photoreactions through energy transfer or through the production of reactive species such as reactive oxygen species (ROS) (Blough and Zepp, 1995; Pelizzetti and Calza, 2002). Natural waters contain various photosensitizers, such as nitrate, iron and dissolved organic matter (DOM). Light-induced reactions by these photosensitizers can generate a suite of ROS, such as singlet oxygen ($^1O_2$), hydrogen peroxide (H_2O_2) and hydroxyl radicals (OH·), which can react with and transform transparent compounds in the aquatic environment (Blough and Zepp, 1995).

1.4.1. Photodegradation of dissolved organic matter

The most important light absorber in seawater is chromophoric dissolved organic matter (CDOM), which is part of the total dissolved organic matter (DOM) pool and characterized as an extremely complex mixture of organic compounds (Clark and Zika, 2000). CDOM absorbs strongly in the UV and short-visible regimes (300–500 nm), a region with significant energy to initiate photochemical processes. DOM in the marine environment has both terrestrial and marine sources. In coastal areas, DOM sources include river inputs and autochthonous biological production (Barrón and Duarte, 2015). However, most DOM in the open ocean is of marine origin, such as *in situ* production by phytoplankton and microbial activity. The terrestrial source only represents ~1% of the total annual total organic carbon input to the ocean (Stein and Macdonald, 2004).

Photochemical transformation of DOM, via either direct or indirect photoreactions, produces CO_2 (complete oxidation), partially oxidized DOM that is more bio-refractory,

and more biolabile low-molecular-weight DOM (Miller and Zepp, 1995; Moran and Zepp, 1996; Johannessen and Miller, 2001; Kaplan and Cory, 2016). The chromophoric fraction of DOM first absorbs solar energy and leads to the generation of photo-excited CDOM. The photo-excited CDOM either undergoes direct decomposition or sequentially interacts with water, dissolved oxygen, or iron (Fe) to produce ROS and organic radicals, which in turn induces the oxidization of CDOM and moieties of uncolored DOM that cannot be directly photodegraded. The more bio-labile DOM can be utilized by microbes and converted to CO_2, a process referred to as coupled photochemical-biological degradation of DOM.

1.4.2. Photodegradation of particulate organic matter

Particulate organic matter (POM) provides another type of chromophores and photochemical substrates in aquatic environments. POM is a mixture of living and non-living phytoplankton, zooplankton, bacteria, and their degradation products and macroscopic aggregates (Pelizzetti and Calza, 2002). In the euphotic zone, the major portion of POM is from phytoplankton (Riley, 1971). POM photochemistry in the ocean has generally received little attention, as particulate organic carbon typically accounts for less than 2% of the total organic carbon. However, POM photochemical processes can be important if there are no corresponding dissolved phase photochemical reactions that take place at a comparable rate. The photoreactivity of the particulate phase is often enhanced when particles, such as hydrophobic, particle-bound pollutants, phytoplankton pigments, and photoreactive metals (e.g., Fe, Cu, Mn), are incorporated into POM. In addition, many particulate-bound pollutants and pigments are photolyzed via a static mechanism that does not involve other reactants either on the particle surface or in the dissolved phase, indicating that particulate photoprocesses may be important under the dilute conditions that exist in seawater (Mopper et al., 2015).

An early study demonstrated that the photodegradation of phytodetrital POM may form cross-linked fluorescent products that transform labile organic matter into refractory DOM in the ocean (Kikugawa and Beppu, 1987). More recent surveys have reported the

photochemical conversion of POM to DOC (Kieber et al., 2006; Mayer et al., 2006, 2009a, 2009b; Riggsbee et al., 2008; Estapa and Mayer, 2010; Pisani et al., 2011; Shank et al., 2011), dissolved organic nitrogen (DON) (Mayer et al., 2009b; Pisani et al., 2011), CDOM (Pisani et al., 2011), CO_2 (Estapa and Mayer, 2010; Riggsbee et al., 2008), and carbon monoxide (Xie and Zafiriou, 2009; Song et al., 2013; Song and Xie, 2017). Some other studies investigated the photobleaching of POM (Mayer et al., 2009b) and photochemical loss of the terrestrial lignin biomarkers in resuspended river and coastal sediments (Mayer et al., 2009a). Mayer et al. (2006) referred to the photochemical conversion of POM into DOM as "photodissolution". It has been posited that photodissolution of resuspended sediments is an important source of DOC in the Cape Fear River estuary in North Carolina (Kieber et al., 2006) and in the Mississippi River (Mayer et al., 2006). Light limitation and temperature are considered to be the key factors controlling photodissolution of resuspended sediments in river and estuarine systems (Mayer et al., 2006).

1.5. PHOTOCHEMICAL TRANSFORMATION OF PLASTICS IN THE MARINE ENVIRONMENT

1.5.1. Photochemical structural transformation

Synthetic plastics are a form of anthropogenic particle in the ocean. Studies on the photochemical transformation of plastics in seawater are scarce, and quantitative surveys of the products of photodegradation of plastics are even more limited. It is reasonable to assume that photodegradation of plastics in seawater involves both direct and indirect photoreactions, similar to the photodegradation of CDOM and POM (Zafiriou et al., 1984; Zafiriou, 2002). Direct photodegradation of plastics requires the presence of light-absorbing moieties (i.e. chromophoric groups) in the plastics to initiate photoreactions. Some plastics, such as the aromatic polymers of PS, polycarbonate (PC), and PET,

contain strong UV-absorbing chromophoric groups (i.e. unsaturated carbon bonds), so they are prone to undergoing direct photodegradation. However, some polymers that do not contain chromophoric groups in their backbone, like PE and PP, may be photodegraded as well if they contain chromophoric impurities (e.g. catalyst residues, certain additives, and organic contaminants) that absorb sunlight and thus induce degradation of polymers by photosensitization.

The rate of indirect plastic photodegradation largely depends upon the sensitizing capacity of the photosensitizer, which results from its concentration, chemical composition, and origin (Galí et al., 2016). Moreover, the photodegradation of plastics is expected to depend on the spectral composition of the incident light, as well as on environmental factors such as water temperature, as observed for certain photochemical processes of CDOM and POM (Zhang et al, 2006; Estapa et al., 2012; Song et al., 2013; Mopper et al., 2015).

Photodegradation may occur in the absence of oxygen (chain breaking or cross-linking) and the presence of oxygen (photooxidative) degradation (Yousif and Haddad, 2013). Since floating plastics on the surface of the sea are exposed to moderate temperatures, oxygen and sunlight are the most important factors to initiate the oxidative degradation of plastics. Commonly used plastics, such as PE, PP and PS, are susceptible to photo-initiated oxidative degradation, which is arguably their most important degradation pathway in the marine environment (Andrady, 2011). Once the chromophoric groups (unsaturated double bonds or external impurities) in the polymers absorb light energy, C-H bonds on the polymer backbone are broken by light to produce free radicals. These free radicals can undergo autoxidation by complex radical reactions in the presence of oxygen, forming oxygen-containing functional groups (Figure 3). This pathway also leads to a decrease or increase in the molecular weight through random chain scission and cross-linking, respectively. The products of radical termination reactions, such as olefins, aldehydes, and ketones are expected to be more susceptible to photodegradation with their unsaturated double bonds. Moreover, the reduced molecular weight makes the polymers

brittle, more easily fragmented, and thus more labile to biodegradation (Gewert et al., 2015).

In terms of polyolefins, PP is less stable than PE, as the tertiary carbon (a carbon atom bound to three other carbon atoms) present in PP is more prone to abiotic attack than the secondary carbon (a carbon atom bound to two other carbon atoms) found in PE. PS is considered to be the most resistant thermoplastic polymer towards biodegradation but is more sensitive to photodegradation with the presence of aromatic rings. Like PP and PE, PVC does not possess chromophores. However, photoreactions initiated by chromophoric impurities can lead to the dechlorination of PVC and then to the formation of conjugated carbon double bonds in a polyene polymer. The unsaturated C=C bonds are unstable to photodegradation, causing the polymer backbone to be degraded into smaller pieces. Thermoplastic polyurethanes (TPUs) are composed of thermoplastic hard segments (aromatic or aliphatic) and elastomeric soft segments (polyether or polyester). TPUs are susceptible to degradation by UV light radiation. The photooxidation of aromatic polyurethane involves the scission of the urethane group and the oxidation of the central methylene group with quinone (yellow) formation as a chromophoric reaction product (Rosu et al., 2009).

1.5.2. Photodissolution

Analogous to the photodissolution of natural POM discussed in section 1.4.2, the photodissolution of synthetic plastics in seawater has recently been reported in a few studies. Tian et al. (2019) observed the production of both CO_2 and DOM from PS nanoplastics suspended in pure water and exposed to UVC radiation (254 nm). Similarly, Ward et al. (2019) found that PS microplastics can be both completely oxidized to CO_2 and partially oxidized to DOC under simulated-solar radiation. L. Zhu et al. (2020) showed that simulated sunlight can convert PE, PP and expanded PS microplastics floating in seawater into DOC, with the expanded PS being the most prone to photodegradation, PE the most photo-resistant, and PP in-between. The latter two studies

suggest that photodissolution may play a crucial role in controlling the lifetime of MPs in the marine environment.

Despite this progress, our knowledge concerning the photodissolution of plastics remains limited. For example, Romera-Castillo et al. (2018) observed a rapid leach of DOC from PE and PP macroplastics under dark conditions but small or negligible effects of solar exposure on this process, a result quite different from those of the studies noted above. This difference could result from different formulations (e.g. plastic additives) of the plastics used (Ward et al., 2019). In addition, earlier studies on MPs photodissolution focused exclusively on large-sized MPs (>2 mm) and carbon-based polymers. Photodissolution of nitrogen-containing polymers, such as TPU, may release dissolved nitrogen in addition to DOC, which may be significant for providing fixed-nitrogen for bacterial and phytoplankton growth. As far as the plastic size is concerned, smaller MPs possess larger surface area to volume ratios and thus receive higher light doses under otherwise identical irradiation conditions. Moreover, while positively buoyant MPs with a size of >1 mm stay at the sea surface, sub-millimeter MPs tend to be dispersed into the subsurface by turbulent mixing (Enders et al., 2015), subjecting the MPs to lower light intensity.

Water temperature is another environmental variable that could affect photodissolution of MPs. While Andrady (2011) argued that temperature is a determining factor in the photodegradation of plastics, Ward et al. (2019) demonstrated that the photooxidation of PS microplastics depended only weakly on temperature. Likewise, little information is available on the effect of spectral composition of the incident light on the photodegradation of MPs, which is important for addressing the depth-dependence of MP photodegradation in the water column (Ward et al., 2019). Without a better appreciation of the effects of these environmental factors, the role of MPs photodissolution in controlling the transformation and fate of MPs remains elusive.

1.6. OBJECTIVES

The overall goal of this project is to advance our knowledge about the photodissolution of MPs in the ocean, with the following specific objectives:

1) To quantify the photodissolution rates of sub-millimeter-sized MPs and expand the target MPs to include nitrogen-containing polymers.

2) To evaluate the effects of temperature and the spectral composition of incident light on the photodissolution rates.

3) To assess the implication of photodissolution for the fate of MPs in the ocean.

2. METHODS

2.1. MICROPLASTICS STUDIED

Five types of MPs were examined: low-density polyethylene (PE), polypropylene (PP), polyvinyl chloride (PVC), polystyrene (PS) and thermoplastic polyurethane (TPU); all of which are analytical grade in purity and spherical in shape with a diameter of 200 μm except for TPU having a diameter of 100 μm. These MPs were purchased from Shanghai Youngling Electromechanical Technology Co., Ltd. TPU has different chemical structures, depending in part on whether the polyurethane is synthesized from aliphatic or aromatic diisocyanates and from short- or long-chain of diols. The structure of the TPU MPs we used is not disclosed by the supplier.

An initial irradiation test confirmed that PE and PVC could not produce significant amounts of DOC within a 7-d time period under the conditions described in sections 2.2 and 2.3.1 and thus were excluded from further study. The remaining three polymers were chosen; their properties and common commercial applications are shown in Table 1.

2.2. SAMPLE PREPARATION

One hundred and forty-seven milligrams of each microplastic type were added to 350 mL of artificial seawater (ASW) contained in a 400-mL jacketed glass beaker. This high concentration of MPs was adopted to accelerate the photoproduction and thus facilitate the quantification of DOM. The ASW was prepared by adding Instant Ocean® Sea Salt to Nanopure water to reach a salinity of ~35 and then filtered through a 0.2-μm polyether sulfone membrane filter to remove any particles including bacteria. The Instant Ocean® Salt-based ASW has a chemical composition very similar to that of natural seawater (Hefner et al., 2006) but contains very low concentration of DOM (CDOM,

absorption coefficient at 254 nm: 0.59 m^{-1}; DOC: 22.8 µmol L^{-1}). Before use, all glassware was soaked with 10% hydrochloric acid (HCl) overnight, thoroughly rinsed with Nanopure water, air-dried, and finally heated at 450°C for 5 hours.

Table 1: Chemical structure, density, and common applications of the selected microplastics (Andrady, 2011; Polymer Properties Database, 2015; Plastics Europe, 2020). The chemical structure of the thermoplastic polyurethane was not disclosed by the supplier.

Plastic class	Molecular structure	Density (g cm^{-3})	Common applications
Polypropylene (PP)	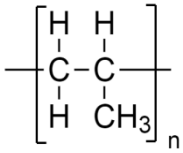	0.91	Food packaging, sweet and snack wrappers, hinged caps, microwave containers, pipes, automotive parts, bank notes, etc.
Polystyrene (PS)	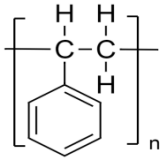	1.05	Food packaging (dairy, fishery), building insulation, electrical and electronic equipment, inner liner for fridges, eyeglasses frames, etc.
Thermoplastic Polyurethane (TPU)	Undisclosed	Undisclosed	Footwear, hydraulic gaskets, synthetic leather, building materials, caster wheels, automotive instrument panels, power tools, gaskets, drive and timing belts, outer cases of electronic devices, and sportswear.

2.3. IRRADIATION

2.3.1. Full-spectrum irradiation

The plastic sample-filled beakers were irradiated in triplicate under a SUNTEST CPS solar simulator equipped with a 1500 W xenon lamp, with a special UV filter installed to remove radiation at wavelength <290 nm (Figure 4). The beakers were covered with a quartz plate and thermostatted by a circulating water bath. The MP suspensions, continuously mixed with a PTFE-coated magnetic stirring bar, were irradiated over a period of seven days. To evaluate the effect of temperature on the photodissolution of microplastics, irradiations were conducted at three different sample temperatures: 10 ± 1, 20 ± 1, and 30 ± 1°C. Blank tests without the addition of the MPs were performed to account for potential loss of DOM in the ASW matrix and potential release of DOM from the PTFE-coated stirring bar. For all irradiations, parallel dark controls were incubated to correct for potential thermal production of DOM from the MPs.

The MP suspension in the beaker was sampled at 1-d intervals using a BD Becton Dickinson 50-mL sterile polypropylene syringe fitted with an acid-cleaned PTFE tube (o.d.: 3.2 mm; i.d.: 2.0 mm). Sampling was performed while the suspension in the beaker was being well mixed so that the suspension was homogenously drawn into the syringe. The syringe and tube were thoroughly flushed with Nanopure water before sample drawing. After sampling, part of the suspension in the syringe was passed through a pre-combusted Whatman GF/F microfiber filter (pore size: 0.7 μm; diameter: 25 mm) contained in a Swinnex polypropylene filter holder; the filtrate collected into a 9-mL glass vial for DOC and dissolved nitrogen (DN) analysis and into a 60-mL pre-combusted clear-glass bottle (~20 mL filtrate) for CDOM absorbance measurement. The remaining part of the suspension was filtered through a 40-μm Falcon Cell Strainer; the filtrate (~4.5 mL) was collected into a 5-mL sterilized plastic vial for heterotrophic bacteria enumeration. DOC/DN samples were acidified to pH ~2 by adding 100 μL of 2 M hydrochloric acid (Reagent grade) to each vial. DOC/DN and CDOM samples were

sealed with PTFE-lined screw caps and stored in the dark at 4°C until analysis within two weeks of sample collection for CDOM and within two months of sample collection for DOC/DN. Bacterial samples were fixed with 0.1% glutaraldehyde and stored at -80°C until analysis. Bacterial abundances were monitored to verify if the axenic conditions were maintained during the incubation period. This monitoring was, however, only performed for selected samples (ASW medium and TPU at 20$^{\circ C}$) due to resource limitation.

At the end of the 7-d irradiation, the MPs remaining in the irradiation vessel were collected onto a Whatman GF/F microfiber filter using the syringe filtration unit described above, rinsed three times with Nanopure water, and then transferred to a 10-mL pre-cleaned glass beaker. The beaker was wrapped with aluminum foil and stored at -80℃ until elemental composition analysis.

In addition to the short-term time-series irradiations, a 60-d fixed-duration irradiation, along with parallel dark controls, was conducted for all three polymers at 30°C using the SUNTEST CPS solar simulator. The MP suspension was sampled at the start and end of the irradiation for DOC/DN measurements. The MPs remaining after the irradiation was collected for elemental composition analysis. Procedures for sampling and sample manipulation were the same as described above.

2.3.2. Effect of light composition

To determine the effect of the spectral composition of the incident light on the photodissolution of MPs, the MP suspensions were irradiated using the SUNTEST CPS solar simulator under three light treatments: full spectrum (290–700 nm), UVA plus visible (320–700 nm), and visible only (400–700 nm), with the latter two treatments being realized by covering the MPs suspensions with a Mylar-D film and a Plexiglas acrylic UF4 light filter, respectively. The Mylar-D film removed most of the UVB (290–320 nm) radiation and the UF4 filter essentially blocked the entire UV (290–400 nm) band (Figure 5). Irradiations lasted for 7 d at 20°C. Samples were taken at the start and end of the

irradiation for DOC and DN measurements according to the procedure described in section 2.3.1.

2.3.3. Photodegradation of MP-derived DOM

An additional full-spectrum irradiation was performed to assess the photodegradability of the DOM photoproduced from PP, PS, and TPU after the 60-d fixed-duration irradiation (section 2.3.1). The post-irradiated MP suspension was filtered through a 0.2-µm polyethersulfone membrane filter. The filtrate was transferred into pre-combusted cylindrical quartz tubes (length: 25.0 cm; i.d.: 2.2 cm). The tubes were immersed in a water bath thermostatted at 30 ± 1°C and exposed to the full-spectrum radiation using a SUNTEST XLS+ solar simulator. The output irradiance spectrum of SUNTEST XLS+ is similar to that of the CPS model (Figure 5A,B) which was unavailable at the time of this experiment. DOC/DN samples were collected in triplicate after 0, 7, and 14 days of irradiation.

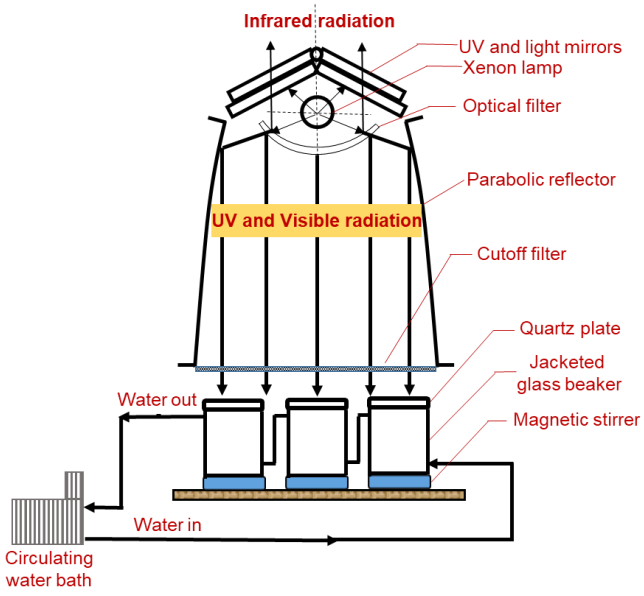

Figure 4: Schematic of the irradiation system employed.

2.4. ANALYSIS

2.4.1. Irradiance

The spectral irradiance reaching the upper surface of the irradiation vessels was measured at 1-nm intervals from 250 to 800 nm, using an OL-756 spectroradiometer fitted with an OL IS-270 2-inch integrating sphere and calibrated with an OL752-10E irradiance standard (Gooch and Housego, USA). The irradiance spectra of the CPS and XLS+ solar simulators under different light-screening conditions are shown in Figure 5A,B. A comparison of the full spectra of the solar simulators with the reference spectrum at 0° latitude (Apell and McNeill, 2019) is shown in Figure 5C.

2.4.2. Absorbance

CDOM absorbance was scanned from 800 to 200 nm at 1-nm intervals using a Perkin-Elmer lambda-35 dual beam UV-visible spectrometer fitted with 5-cm quartz cells and referenced to Nanopure water. Samples were warmed to room temperature before analysis. The absorption coefficient of CDOM, $a_{CDOM}(\lambda)$ (m^{-1}), where λ is wavelength in nanometers (nm), was calculated as 2.303 times the absorbance divided by the light pathlength of the cells in meters (0.05 m). A baseline correction was applied by subtracting the average absorbance between 683 and 687 nm from all spectral values (Babin et al., 2003). The lower detection limit of a_{CDOM} measurement, defined as three times the standard deviation of five replicate blank measurements of Nanopure water, was estimated to be 0.022 ± 0.005 m^{-1} (mean ± SD) in the wavelength range from 250 to 700 nm. The mean relative standard deviation of the measurements of five sets of triplicate irradiated samples was 6% ± 2% at 254 nm.

The absorption coefficient at 254 nm, $a_{CDOM}(254)$, was chosen to be the indicator of the abundance of CDOM, as in some other studies (Laudon et al., 2004; Shao et al., 2016). This wavelength was chosen due to the higher accuracy of absorbance

measurement at short UV wavelengths than at the longer UV and visible wavelengths. Moreover, CDOM photoproduced from the MPs tested in this study showed rather weak absorption at the longer UV and visible wavelengths (section 3.5). For brevity, the symbol $a_{CDOM}(254)$ will be shortened to a_{254} hereinafter.

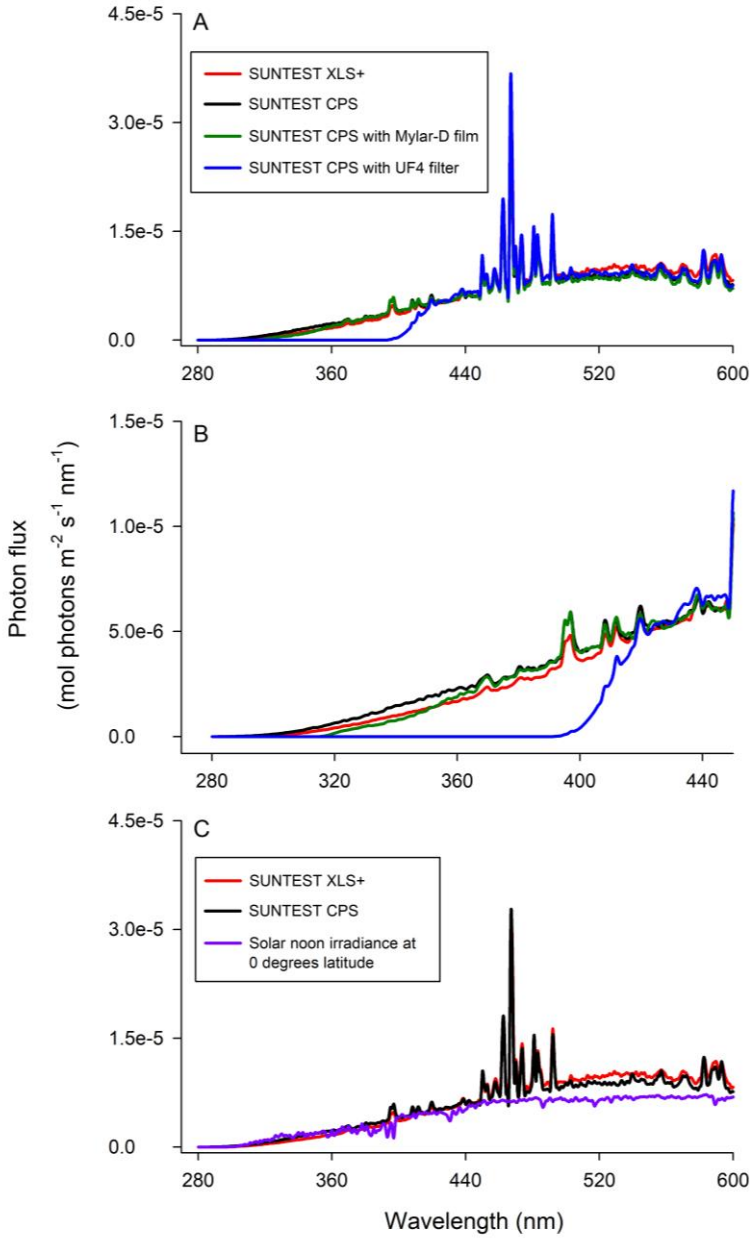

Figure 5: (A) Irradiance spectra (280–600 nm) of the SUNTEST CPS and XLS+ solar simulators. (B) A closeup view of panel A in the wavelength range from 280 to 450 nm. (C) A comparison of the irradiance spectra of the solar simulators with the reference irradiance spectrum at 0° latitude on June 21st (Apell and McNeill, 2019). In panels A and B, Mylar-D: spectrum screened by the Mylar-D film; UF4: spectrum screened by the Plexiglas acrylic UF4 filter.

2.4.3. DOC and DN

The DOC concentration ([DOC]) was measured using a Shimadzu TOC-Vcpn carbon analyzer equipped with a TNM-1 module (Total Nitrogen Measurement unit) simultaneously measuring the dissolved nitrogen concentration ([DN], inorganic plus organic). Potassium hydrogen phthalate and potassium nitrate were used to standardize [DOC] and [DN] measurements, respectively. In addition, samples were systematically checked against Nanopure water (Barnstead Nanopure Infinity) and St. Lawrence Estuary seawater secondary reference water (86.7–95.0 µmol C L^{-1} and 19.3–20.7 µmol N L^{-1}) every seventh sample analysis. The secondary standard was referenced to deep Sargasso Sea reference water (42–45 µmol C L^{-1} and 31-33 µmol N L^{-1}) produced by the Hansell's consensus reference materials (CRM) program. The coefficient of variation on three replicate injections was typically <2% for DOC and <5% for DN.

2.4.4. Bacteria abundance

Free-living heterotrophic bacterial abundance was determined using an Epics Altra flow cytometer (Beckman Coulter) equipped with a 488 nm argon laser operated at 15 mW (Belzile, 2008). A 0.5 mL subsample was half diluted in 1×Tris-EDTA buffer (pH 8) and the resulting 1 mL solution was incubated with 0.25 µL SYBR Green I (Ci = 10 000×, Invitrogen) for 30 min at room temperature in the dark. Ten milliliters of fluorescent beads (1 µm in diameter; Fluoresbrite Plain, YG) were added to each sample as an internal standard and then the samples were analyzed with the cytometer for 3 min. Bacterial cell abundance was calculated from the analysis volume that had been gravimetrically determined and corrected for the dead volume (50 µL, i.e. the volume taken from the sample tube but not accounted for when data acquisition was stopped).

2.4.5. Elemental compositions

The carbon (C) and nitrogen (N) contents of the MPs were determined using a Carlo Erba NC2500 elemental analyzer following the procedure reported by Hélie (2009). Briefly, The MPs samples were dried for 24 hours using a Freeze dry system LABCONCO equipped with a FreeZone 6 Liter Model (Temperature: -40°C, Vacuum: (14 ± 2) ×10-3 mbar) before analysis. The weighed samples (1–2 mg) were wrapped in a tin or silver catalyst and then dropped from a sequential carousel into an oven simultaneously injected with oxygen. Combusted at ~1000°C in the oven, the samples were oxidized and converted into gases. The resulting gases were reduced by copper wires kept at 800°C and separated chromatographically to allow determination of the amounts of individual gases on a thermal conductivity detector. The method for oxygen (O) content analysis is essentially the same except that: 1) an Elementar Vario PyroCube elemental analyzer was employed; 2) pyrolysis in a glassy carbon reactor at 1450°C was used instead of combustion; 3) the resulting gases were separated in a chemical trap instead of a chromatographic column.

2.4.6. Statistics

Two-tailed t-tests were performed to determine the significance of difference between the two sample groups (e.g. light vs. dark). Statistical analyses and graph production were carried out using Microsoft Office 365 and SigmaPlot 10.0.

3. RESULTS AND DISCUSSION

3.1. ELEMENTAL COMPOSITION OF MPs

The percent C, O, and N contents of the MPs are shown in Table 2. The presence of minor O in the original PP and PS suggests that these MPs contained O-containing impurities and/or were partially oxidized during storage. The atomic C/O ratios of PP and PS decreased dramatically under light exposure (Table 2), indicating the occurrence of photooxidation of these polymers, which is consistent with the results of earlier studies (Tang et al., 2019; Tian et al., 2019; L. Zhu et al., 2020). Interestingly, the C/O ratio in the dark controls also substantially decreased, albeit with lower rates compared to the light treatments. This observation demonstrates that PP and PS underwent thermal oxidation and/or hydrolysis during the dark incubation (Gewert et al., 2015), although dark DOC production from these polymers was marginal (section 3.3). For TPU, the C/O ratio only slightly decreased during incubation in both the dark (<6%) and light (<9%). The C/N ratio for the dark control dropped moderately, by 11% on day 7 and 16% on day 60. The C/N ratio for the light treatment remained unchanged on day 7 but increased by 49% on day 60, indicating a preferential loss of nitrogen relative to carbon during the prolonged exposure.

Table 2: Changes of the elemental compositions of MPs during light and dark incubations at 30 °C. Percent contents are on a w/w basis. C/O and C/N represent the atomic ratios of C to O and C to N, respectively. “Original” refers to MPs not in contact with the artificial seawater medium. PP: polypropylene; PS: polystyrene; TPU: thermoplastic polyurethane.

		PP			PS			TPU			
	Time (d)	%C	%O	atomic C/O	%C	%O	C/O	%N	%C	%O	C/O	C/N
	Original	83.86	0.31	356.1	87.52	0.19	614.2	0.702	59.30	30.58	2.59	98.6
Light	7	77.18	3.16	32.6	82.26	1.19	92.6	0.673	56.65	31.01	2.44	98.2
	60	69.24	5.99	15.4	66.93	10.22	8.7	0.408	51.34	29.20	2.34	147.0
	Original	83.86	0.31	356.1	87.52	0.19	614.2	0.702	59.30	30.58	2.59	98.6
Dark	7	78.49	0.77	136.8	77.92	1.56	66.7	0.715	53.97	28.27	2.55	88.1
	60	75.72	1.49	67.7	81.80	1.22	89.6	0.726	51.50	28.40	2.42	82.7

3.2. BACTERIAL ABUNDANCE AND ASW BLANKS

Bacterial cell abundances were below the detection limit (~1×10^4 cells mL^{-1}), suggesting that bacteria did not significantly grow over the experimental durations (Fig. S1). [DOC], [DN], and a_{254} in the ASW medium were rather stable or only slightly fluctuated over the time-course incubations under both the dark and light conditions (Fig. S2). No significant differences were observed on most occasions between the light and dark treatments (p >0.1). These results indicate that contamination from the PTFE stirring bars in the irradiation vessels was negligible and that the very low DOM in the original ASW medium ([DOC] = 22.8 ± 6.3 μmol L^{-1}; a_{254} = 0.59 ± 0.07 m^{-1}) was resistant to photodegradation.

3.3. DARK PRODUCTION OF DOC, CDOM, AND DN

[DOC]s on day zero in the PP and PS samples only differed slightly (PP: -23.4–16.8%; PS: -17.6–9.3%) from those in the ASW medium; a_{254} behaved similarly (Table 3). In contrast, the day-zero [DOC]s in the TPU sample increased by more than two times at 10℃ and 20℃ and by seven times at 30℃ compared to those in the ASW medium; a_{254} also augmented by 2.5 times at 10℃ and 4.4 times at 30℃. As the day-zero sampling was performed within 30 minutes of the MPs addition, the rapid increases in [DOC] and a_{254} must have resulted from immediate leaching of DOM from TPU. Given that the changes in [DN] were minor and inconsistent in direction at different temperatures (-10.2–30.1%), the leaching was likely associated with certain carbon-based additives in the MPs rather than from the pure TPU polymer itself. DOC and CDOM continued to be leached out rapidly during day 1 at 10℃ and 20℃ but not at 30℃, as demonstrated by the temporal [DOC] and a_{254} trends in the dark controls (Figure 6G,H, Figure 7G,H), indicating that the leaching at 30℃ was essentially completed within 30 minutes.

The cumulative [DOC] and a_{254} from day 0 to day 1, 188.7 μmol L^{-1} and 3.35 m^{-1} at 10℃ and 183.4 μmol L^{-1} and 3.24 m^{-1} at 20℃, were comparable to those on day 0 at 30℃ ([DOC]: 189.1 μmol L^{-1}; a_{254}: 3.37 m^{-1}) (Table 3). Therefore, although the leaching occurred much faster at 30℃, the total amounts of DOC and CDOM leached out were similar at the three different temperatures. From day 1 onward, [DOC] remained approximately constant or only slightly fluctuated at the two lower temperatures but steadily crept up at 30℃ (Figure 6G-I), with a net accumulation of 40.6 μmol L^{-1} on day 7 and 172.9 μmol L^{-1} on day 60. a_{254}, however, remained fairly stable after the initial leaching at all three temperatures (Figure 7G-I). No significant production of DN was observed in the dark controls of TPU at any of the three temperatures (Figure 10). This was consistent with the reduced C/N ratio of the remaining TPU MPs in the dark control at 30℃ (Table 2); wherein DOC was produced but DN was not. The production of DOC without concurrent increases in a_{254} or [DN] indicates that the DOC originated from a

transparent precursor free of nitrogen which could not be the pure TPU polymer itself or the chromophore-containing additives mentioned earlier.

[DOC]s in the dark controls of PP and PS climbed slowly with time, albeit with some fluctuations (Figure 6A-F). At the end of the 7-d incubations, [DOC] in PP had increased by 4.2 μmol L^{-1} at 10°C, 2.3 μmol L^{-1} at 20°C, and 4.7 μmol L^{-1} at 30°C; the corresponding increases in PS were 5.6 μmol L^{-1}, 2.5 μmol L^{-1}, and 7.1 μmol L^{-1}. The extended 60-d incubations at 30°C did not lead to further increases in [DOC], suggestive of a cessation of the dark DOC production somewhere between 7 and 60 d. Unlike [DOC], a_{254} for the dark controls of PP and PS did not show significant increases (Figures 7A-F), indicating no production of CDOM under the dark conditions.

The instant leaching of DOC by TPU seen in this study is similar to the behavior that Romera-Castillo et al. (2018) observed for some postconsumer plastic products of PE and PP. These researchers further confirmed that the PE- and PP-leached DOC could be readily consumed by marine microbes and suspected that plastics-leached DOC might have the potential to stimulate microbial activity on global ocean scales. Our results here, however, show that the leaching of DOC from PP and PS under dark conditions is slow, marginal, and unsustainable. It could be that certain plastic additives were mainly responsible for the important DOC leach observed by Romera-Castillo et al. (2018), whereas the PP and PS products used in our study plausibly contained little leachable additives. Therefore, the leaching behavior of plastics likely relies on the nature and content of additives incorporated into the host plastics, complicating attempts to scale up laboratory results based on limited types and formulations of plastics tested.

Table 3: Day-zero [DOC], a_{254}, and [DN] in the artificial seawater (ASW) medium and microplastic suspensions of polypropylene (PP), polystyrene (PS), and thermoplastic polyurethane (TPU). %change = (MPs-ASW)/ASW × 100. A positive %change indicates an increase relative to the original artificial seawater solution, while a negative %change denotes a decrease.

	[DOC] (µmol L^{-1})			a_{254} (m^{-1})			[DN] (µmol L^{-1})		
	10℃	20℃	30℃	10℃	20℃	30℃	10℃	20℃	30℃
ASW	20.9 ± 1.3	25.1 ± 2.2	23.7 ± 0.9	0.56 ± 0.05	0.52 ± 0.08	0.62 ± 0.05	7.9 ± 0.9	6.4 ± 0.2	7.8 ± 0.5
PP	24.4 ± 1.1	19.2 ± 1.5	23.3 ± 1.3	0.64 ± 0.07	0.58 ± 0.19	0.58 ± 0.03	8.0 ± 0.3	5.2 ± 0.1	7.3 ± 0.3
PS	22.8 ± 1.9	20.6 ± 2.9	25.2 ± 0.7	0.48 ± 0.03	0.45 ± 0.05	0.60 ± 0.04	8.8 ± 1.2	4.8 ± 0.2	8.3 ± 0.1
TPU	81.9 ± 5.0	85.6 ± 1.7	189.1 ± 4.5	1.98 ± 0.11	2.21 ± 0.39	3.37 ± 0.13	8.6 ± 0.3	5.7 ± 0.1	10.1 ± 0.8
PP %change	16.8	-23.4	-1.5	14.1	12.1	-7.5	1.4	-19.1	-5.5
PS %change	9.3	-17.6	6.4	6.6	-13.0	-22.4	11.0	-24.5	7.3
TPU %change	292.4	241.7	699.7	254.7	327.2	441.2	8.4	-10.2	30.1

3.4. PHOTOPRODUCTION OF DOC

Under full-spectrum irradiation, DOC concentrations in all MPs samples at all three temperatures increased exponentially over the 7-d exposure period (Figure 6, Table 4). The DOC production in the light treatments exceeded that in the dark controls, with the difference becoming increasingly larger with the irradiation time. At the end of the 7-d exposure, the production of DOC in PP reached 32.0 μmol L^{-1} at 10°C, 36.1 μmol L^{-1} at 20°C, and 180.3 μmol L^{-1} at 30°C, with the corresponding values of 28.6 μmol L^{-1}, 24.3 μmol L^{-1}, and 72.0 μmol L^{-1} for PS and of 113.4 μmol L^{-1}, 237.0 μmol L^{-1}, and 606.6 μmol L^{-1} for TPU. During the 60-d fixed-duration exposure at 30°C, [DOC] increased by 3168.0 μmol L^{-1}, 6027.6 μmol L^{-1}, 3959.2 μmol L^{-1} in PP, PS, and TPU, respectively, which are 18, 84, and 6 times those produced over the 7-d period at the same temperature. The values obtained from the 60-d irradiations are, however, negligible compared to the unrealistically high values (orders of magnitude of 10^{11}–10^{17} μmol L^{-1}) expected from the exponential-growth equations derived from the 7-d irradiations, indicating that the exponential increase in the DOC photoproduction seen during the short-term irradiation was unsustainable. To compare the efficiencies of photochemical conversion of plastic carbon into DOC among the three polymers, the DOC photoproduced during the 60-d irradiation was normalized to the initial plastic carbon mass contained in each of the polymer samples, yielding percent carbon conversion values of 10.8% for PP, 19.7% for PS, and 19.1% for TPU. The higher percent conversion values for PS and TPU could be due to the fact that PS contains aromatic moieties and TPU possesses carbonyl groups and aromatic moieties (if our TPU samples are aromatic diisocyanates-based) while PP has a saturated aliphatic structure (Table 1). Aromatic rings and carbonyl groups can absorb UV and visible radiation and are thus more prone to photolysis than saturated aliphatic structures. The smaller size of TPU (100 μm vs. 200 μm for PP and PS, section 2.1), which led to a higher surface area to volume ratio, could also have contributed to the relatively higher conversion rate of this polymer.

The exponential increase in the photoproduction of DOC observed here is in accordance with the behavior of the larger-sized (~3 mm) postconsumer MPs of polyethylene, PP, and expanded PS (L. Zhu et al., 2020). This phenomenon has been mainly attributed to the accumulation of photoreactive oxygen-containing functional group, particularly carbonyls and hydroperoxides, within the plastics being irradiated (Lacoste et al., 1993; Tidjani, 1997; Gwert et al., 2015; L. Zhu et al., 2020) and to the photofragmentation of the plastics leading to larger surface areas available to absorb light (Lambert and Wagner, 2016; L. Zhu et al., 2020). With the increasing extent of oxidation, the accumulation rate of the photoreactive moieties appears to slow down over prolonged light exposure, as reflected by the lower-than-expected DOC production observed for the 60-d irradiation.

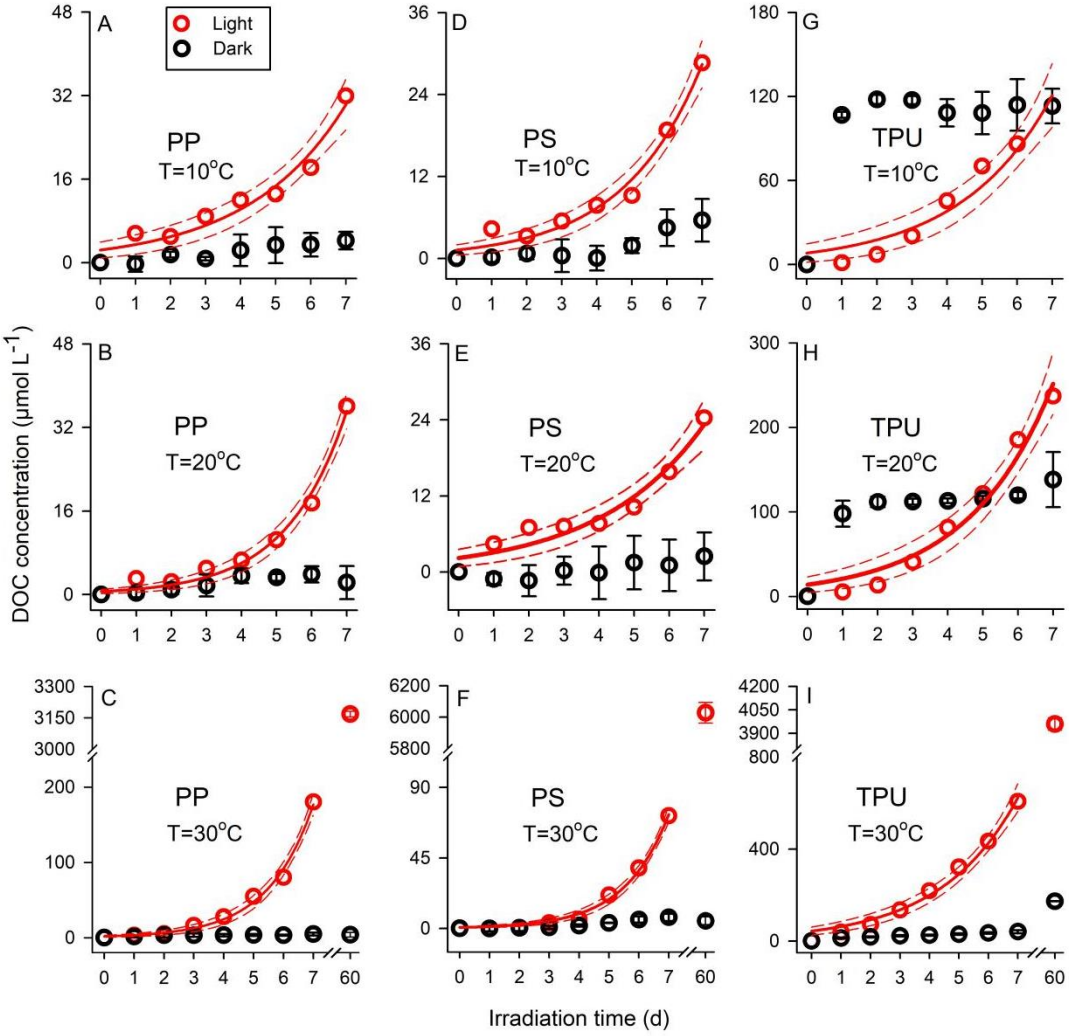

Figure 6: Photoproduction of DOC from different microplastics at different temperatures under full-spectrum irradiation. Data for dark controls are shown as the measured value at each sampling point minus the time-zero value, while data for light treatments represent the measured value at each sampling point minus the corresponding dark control value. Data for the light treatments is fitted to the 2-parameter exponential growth model (solid line; see fitted equations in Table 4). Dashed lines bracket the 95% confidence intervals. Error bars for dark controls are one standard deviation of triplicate incubations. PP: polypropylene; PS: polystyrene; TPU: thermoplastic polyurethane. Note scale breaks in panels C,F, and I.

3.5. PHOTOPRODUCTION OF CDOM

Based on the time-course evolution of a_{254} during the 7-d irradiation period, photoproduction of CDOM from PP was observed at 30℃ but not 10℃ and 20℃, while PS and TPU photochemically generated CDOM at all three temperatures (Figure 7, Table 4). Similar to [DOC], a_{254} also increased exponentially with irradiation time, with net gains at the end of irradiation of 0.87 m^{-1} in the PP sample (30℃); 0.84 m^{-1} (10℃), 1.16 m^{-1} (20℃), and 1.02 m^{-1} (30℃) in the PS sample; 3.26 m^{-1} (10℃), 11.33 m^{-1} (20℃), and 21.93 m^{-1} (30℃) in the TPU sample. TPU was the most prolific CDOM producer followed by PS and PP.

Given that DOC was photoproduced from PP at all three temperatures, the observation of CDOM photoproduction from this polymer only at 30℃ indicates a strong temperature-dependence of CDOM photoproduction and a fundamentally different mechanism for DOM photoproduction at 30℃: the DOM produced at 10°C and 20°C was essentially transparent but at 30°C it contained a chromophoric component. Here we use the [DOC]-normalized a_{254}, i.e., the specific UV absorption coefficient at 254 nm ($SUVA_{254}$), to characterize the photoproduced DOM; $SUVA_{254}$ is an indicator of the aromaticity of DOM (Weishaar et al., 2003). The aromaticity of the photoproduced DOM tends to increase during irradiation at lower temperatures (PS at 10°C and 20°C; TPU at 10°C) and remain relatively stable (PP at 30°C; TPU at 20°C and 30°C) or even decrease (PS at 30°C) at higher temperatures (Figure 8). Such a pattern could arise from the temperature-dependence of the photochemical formation and/or modification of the plastic aromatic precursors for the DOM. Alternatively, it could be due to the enhanced photobleaching of the aromatic moieties in the DOM at higher temperatures. The latter explanation for the near-exponential decay of the $SUVA_{254}$ for the PS-derived DOM at 30℃ is supported by the fact that the DOM thus produced underwent photodegradation when exposed to solar-simulated radiation (section 3.9). Temperature-dependence of photobleaching is known for CDOM occurring in natural waters (Song et al., 2017; X. Zhu et al., 2020). The $SUVA_{254}$ for the PP-derived DOM is substantially lower than those

for the PS- and TPU-derived DOM (Figure 8), which is consistent with the presence of aromatic moieties in the backbones of PS and TPU but not in that of PP. The photoproduction of aromatic DOM from PP should be associated with the presence of intra-polymer chromophoric impurities or structural abnormalities (Gewert et al., 2015), at least during the initiation of the PP photooxidation.

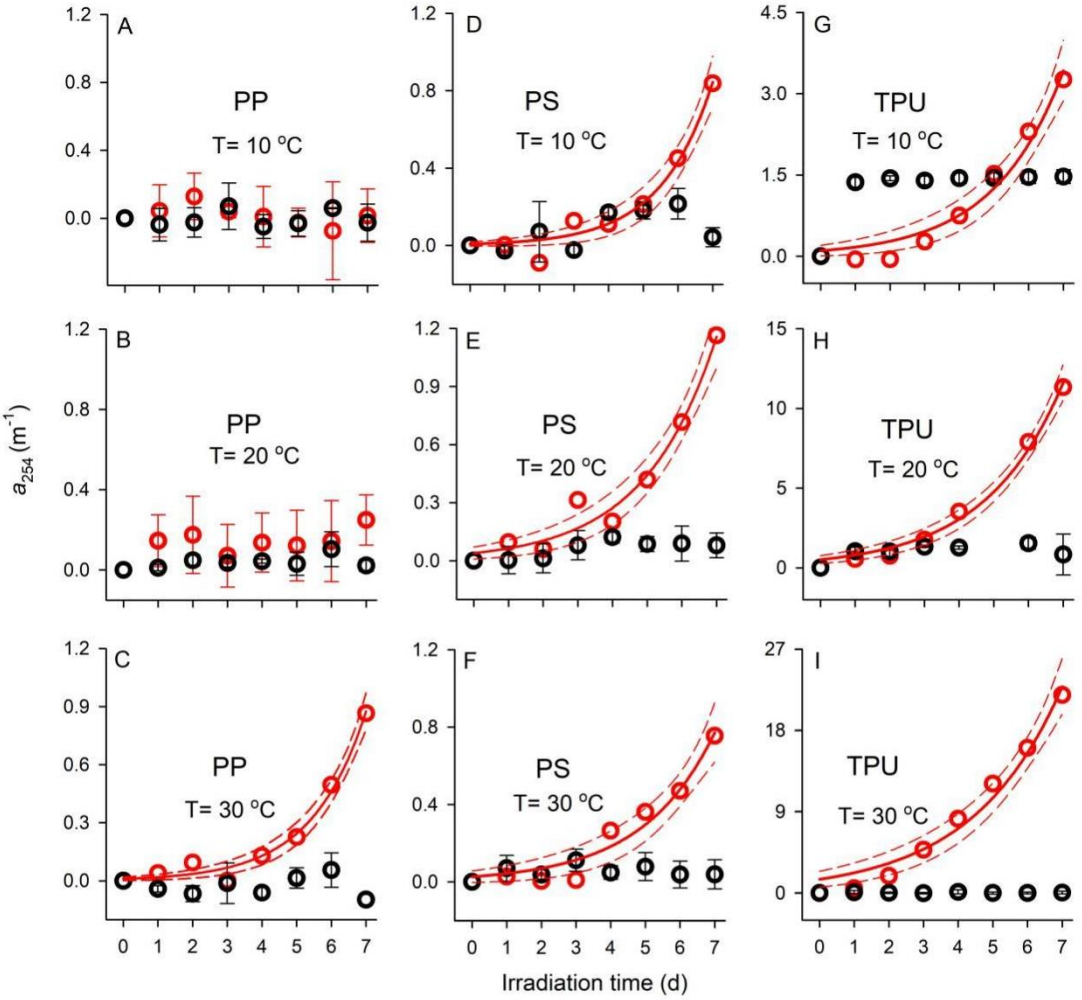

Figure 7: Photoproduction of CDOM from different microplastics at different temperatures under full-spectrum irradiation. Data for dark controls are shown as the measured value at each sampling point minus the time-zero value, while data for light treatments represent the measured value at each sampling point minus the corresponding dark control value. Data for the light treatments is fitted to the 2-parameter exponential growth model (solid line; see fitted equations in Table 4). Dashed lines bracket the 95% confidence intervals. Error bars for dark controls are one standard deviation of triplicate incubations. PP: polypropylene; PS: polystyrene; TPU: thermoplastic polyurethane. The abundance of CDOM is represented by CDOM absorption at 254 nm (a_{254}).

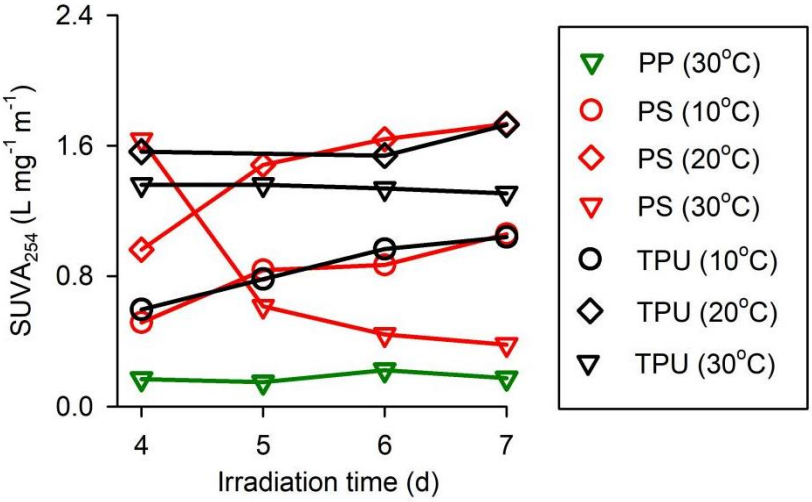

Figure 8: $SUVA_{254}$ of PP, PS and TPU during light incubations at different temperatures. To conform to the conventional practice, $SUVA_{254}$ is based on the decadic (i.e. base 10) absorption coefficient (m^{-1}) and [DOC] in mg L^{-1} and thus has units of L m^{-1} mg^{-1}. The $SUVA_{254}$ data for the first three days of irradiation were discarded due to larger errors associated with the small amounts of DOC and CDOM produced (Figures 6 and 7). PP: polypropylene; PS: polystyrene; TPU: thermoplastic polyurethane.

A characteristic absorption peak centered at 292 nm started to appear on day 4 in the light treatment of PP at 30℃ (Figure 9A), with the peak height increasing exponentially with irradiation time ($y = -0.719 + 0.188*\exp(0.361*x)$, $R^2 = 0.998$, $p = 0.044$). The center wavelength of this peak is about the same as those for aliphatic ketones (Yujing and Mellouki, 2000), which are among the proposed products of photooxidation of PP (Wu et al., 2021). The lack of this peak in the dark (Figure 9A) and prior to day 4 in the light suggests that the relevant products did not result from leaching of a specific UV-absorbing additive. Instead, the compound was plausibly produced after the MPs became sufficiently photooxidized (section 3.1). For TPU, a UV-absorption shoulder was detected in both the dark and light treatments throughout the 7-d incubation at all three temperatures (Figure 9B-D). Although the absorption spectra, particularly those in the light treatments, shifted upwards during the incubation due to an increase in the background CDOM, the size of the shoulder remained relatively stable and did not manifest a substantial difference between the dark and light, implying that the compound associated with this absorption shoulder mainly resulted from the leaching of a UV-absorbing additive from the microplastics upon their contact with the ASW medium. The wavelength of the shoulder, defined as the wavelength at which the shoulder having the maximum height, remained constant in the dark controls (271 nm) but blue-shifted by up to 15 nm from 271 nm to 256 nm during irradiation. This blue-shift could be caused by a change in the substitute groups attached to the UV-absorbing chromophore (e.g. an aromatic ring) or by a decrease in the conjugation of the chromophore (Kalsi, 2007). No conspicuous absorption peaks were detected during the incubation of PS (data not shown), which is consistent with the results of Tian et al. (2019).

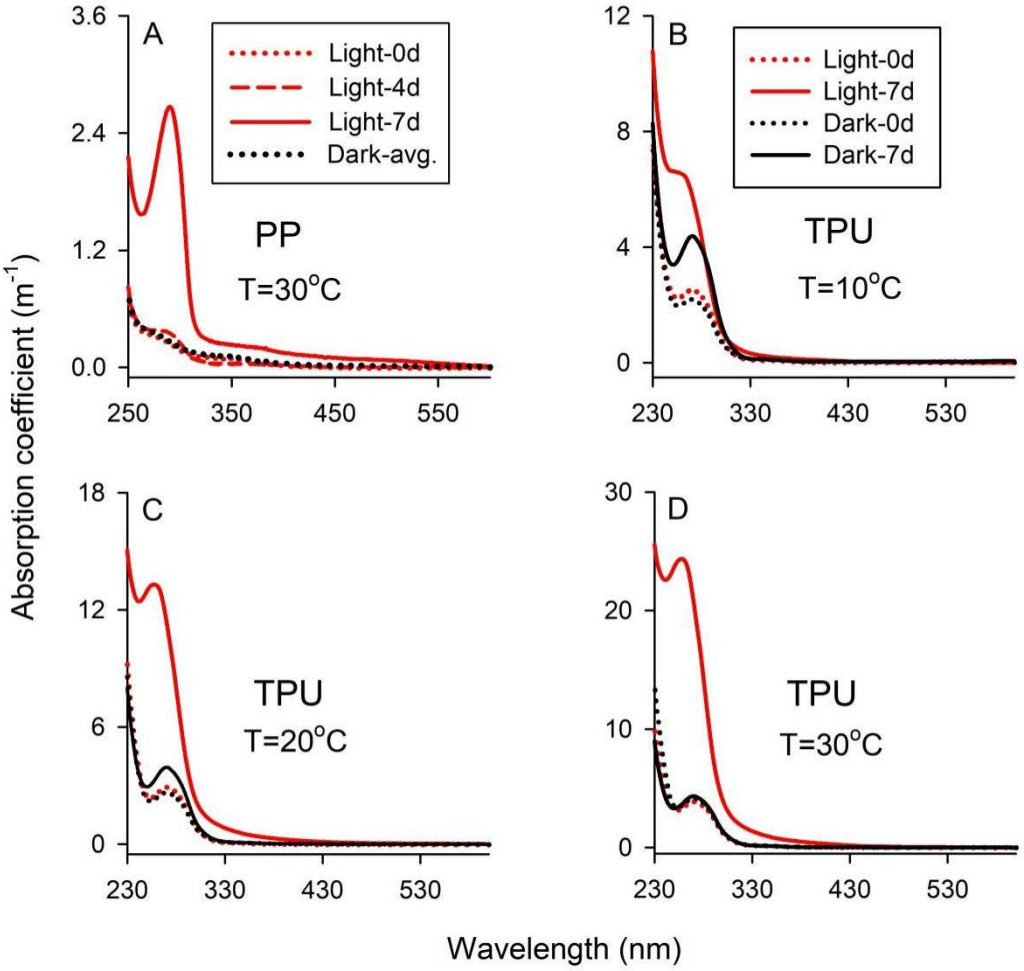

Figure 9: Selected absorption spectra of CDOM derived from PP and TPU during dark and light incubations at different temperatures. Dark-avg: average spectrum for the dark control. PP: polypropylene; TPU: thermoplastic polyurethane.

3.6. PHOTOPRODUCTION OF DN

Photoproduction of DN from TPU was observed at all three temperatures, again in an exponential growth manner (Figure 10, Table 4). The use of the terminology DN (dissolved nitrogen) instead of DON (dissolved organic nitrogen) is because the possibility of photoproduction of dissolved inorganic nitrogen (DIN) from the TPU-derived DON cannot be excluded. It is known that nitrite and/or ammonium can be produced from photodegradation of natural dissolved and particulate organic matter (Bushaw et al., 1996; Kieber et al., 1999; Mayer et al., 2009b; Xie et al., 2012). Over the 7-d exposure period, [DN] increased by 5.6, 14.6, and 29.3 μmol L^{-1} at 10, 20, and 30℃, respectively (Figure 10). The 60-d irradiation at 30℃ generated 165.8 μmol L^{-1} of DN, 5.6 times that produced in 7 days. Similar to [DOC], the photoproduced [DN] after the 60-d irradiation was far smaller than that calculated from the exponential-growth equation derived from the 7-d irradiation (1.65×10^{11} μmol L^{-1}). The percent conversion of the plastic nitrogen into DN reached 78.7% after the 60-d irradiation, a value that is four times the corresponding carbon conversion rate (19.1%, section 3.4). This result demonstrates that nitrogen was preferentially photo-released over carbon, which is consistent with the large increase in the C/N ratio for the post-irradiated TPU (section 3.1, Table 2).

Given the fairly large share of polyurethane plastics (8.2%) in the total non-fiber plastic production worldwide (Geyer et al., 2017) and the increasing usage of other types of N-containing plastics such as styrene-acrylonitrile and acrylonitrile-butadiene-styrene copolymers (Dong et al., 2001), the DN photoproduction from TPU observed here suggests that N-containing plastic wastes may be a potentially significant biolabile nitrogen source for bacterial and phytoplankton growth and may contribute to eutrophication in aquatic environments highly polluted with N-containing plastics. Future studies should be directed at examining the DN production potentials of other N-containing polymers, identifying the chemical species of the DN produced, and elucidating its microbial lability.

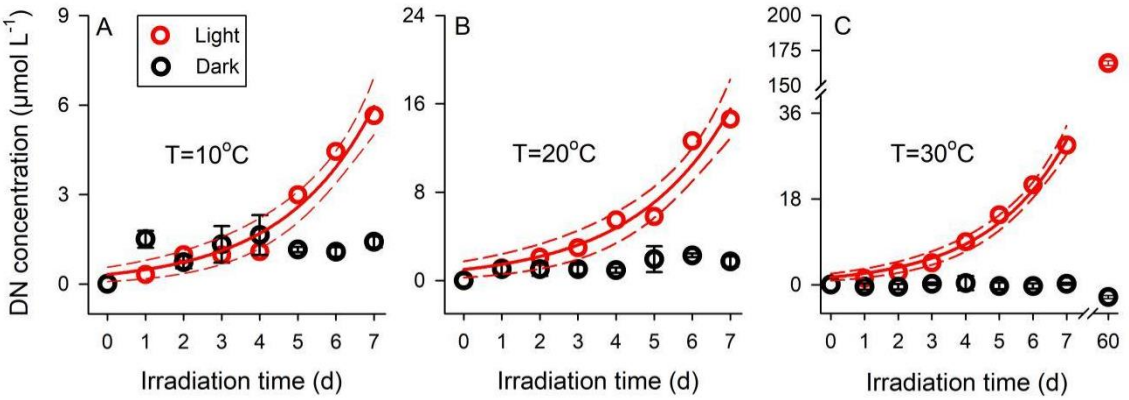

Figure 10: Photoproduction of total dissolved nitrogen (DN) from TPU at different temperatures under full-spectrum irradiation. Data for dark controls are shown as the measured value at each sampling point minus the time-zero value, while data for light treatments represent the measured value at each sampling point minus the corresponding dark control value. Data for the light treatments is fitted to the 2-parameter exponential growth model (solid line; see fitted equations in Table 4). Dashed lines bracket the 95% confidence intervals. Error bars for dark controls are one standard deviation of triplicate incubations. TPU: thermoplastic polyurethane. Note scale breaks in panel C.

Table 4: Equations and statistics describing the kinetics of photorelease of DOC, DN, and CDOM (represented by a_{254}) from the tested microplastics irradiated at different temperatures. The data are fitted to the 2-parameter exponential growth model: Y = a*exp(b*X), where Y stands for [DOC] (µmol L^{-1}), [DN] (µmol L^{-1}), or a_{254} (m^{-1}) and X for irradiation time in days. DOC: dissolved organic carbon; DN: dissolved nitrogen; CDOM: chromophoric dissolved organic matter; a_{254}: absorption coefficient of CDOM at 254 nm; PP: polypropylene; PS: polystyrene; TPU: thermoplastic polyurethane.

Microplastics	Temperature (°C)	a ± SE	b ± SE	R^2	p
DOC					
PP	10	2.42 ± 0.62	0.36 ± 0.04	0.956	<0.0001
	20	0.58 ± 0.17	0.59 ± 0.04	0.987	<0.0001
	30	1.76 ± 0.49	0.66 ± 0.04	0.991	<0.0001
PS	10	1.23 ± 0.31	0.45 ± 0.04	0.978	<0.0001
	20	2.22 ± 0.56	0.34 ± 0.04	0.948	<0.0001
	30	0.62 ± 0.16	0.68 ± 0.04	0.994	<0.0001
TPU	10	8.22 ± 2.68	0.38 ± 0.05	0.950	<0.0001
	20	13.89 ± 3.79	0.41 ± 0.04	0.971	<0.0001
	30	43.41 ± 7.19	0.38 ± 0.03	0.986	<0.0001

DN					
	10	0.32 ± 0.10	0.42 ± 0.05	0.963	<0.0001
TPU	20	0.99 ± 0.30	0.39 ± 0.05	0.956	<0.0001
	30	1.57 ± 0.30	0.42 ± 0.03	0.986	<0.0001
a_{254}					
PP	30	0.01 ± 0.00	0.64 ± 0.05	0.985	<0.0001
	10	0.01 ± 0.00	0.67 ± 0.08	0.970	<0.0001
PS	20	0.04 ± 0.01	0.48 ± 0.05	0.972	<0.0001
	30	0.03 ± 0.01	0.48 ± 0.07	0.950	<0.0001
	10	0.10 ± 0.04	0.50 ± 0.06	0.967	<0.0001
TPU	20	0.51 ± 0.10	0.45 ± 0.03	0.990	<0.0001
	30	1.52 ± 0.36	0.39 ± 0.04	0.973	<0.0001

3.7. TEMPERATURE-DEPENDENCE OF PHOTOPRODUCTION OF DOC, CDOM, AND DN

The photoproduction rates of DOC (P_{DOC}), CDOM (represented by a_{254}, P_{CDOM}), and DN (P_{DN}) were calculated as the first derivatives of the respective concentration-*vs.*-time equations shown in Table 4. As [DOC], a_{254}, and [DN] all increased exponentially with irradiation time (Figures 6,7,10, Table 4), so did their production rates (Figure S3). To examine the temperature effect and its potential temporal variation, the ratios of the production rates at 20℃ and 30℃ to that at 10℃ are plotted against the irradiation time for each of the three production terms (Figure 11).

P_{DOC} in PP (P_{DOC}-PP) showed little difference between 10℃ and 20℃ before day 4 (< 4%) but was 89% higher at 20℃ than at 10℃ on day 7 (Figure 11). P_{DOC}-PP at 30℃ increased more rapidly relative to 10℃, with the rate at 30℃ being 337% higher on day 4 and 970% higher on day 7.

A rapid-rise trend was also observed for the 30℃/10℃ ratio of P_{DOC} in PS (P_{DOC}-PS); the rate at 30℃ exceeded that at 10℃ by 94% on day 4 and by 288% on day 7 (Figure 11B). The 20℃/10℃ ratio of P_{DOC}-PS, however, gradually decreased with irradiation time, leading to P_{DOC}-PS at 20℃ being 39% lower than at 10℃ on day 7. As DOC photoproduced from PS was photomineralizable (section 3.9) and DOM photodegradation is known to be temperature-dependent (Hong et al., 2014; Song et al., 2017), the opposing trends between the 30℃/10℃ and 20℃/10℃ ratios were likely caused by varying degrees of the temperature-dependences of DOC photoproduction from PS and the simultaneous photomineralization of the DOC produced. In the case of 30℃ *vs.* 10℃, the increase in DOC photoproduction resulting from the temperature rise could have outcompeted the enhancement in DOC photomineralization, whereas the balance could have tilted to the latter in the case of 20℃ *vs.* 10℃. Regarding P_{CDOM} in PS (P_{CDOM}-PS), fast decreasing trends were observed for both the 20℃/10℃ and 30℃/10℃ ratios and, somewhat unexpectedly, P_{CDOM}-PS at 30℃ was constantly lower than at 20℃ over the entire 7-d period (Figure 11D). This “abnormality” suggests that

the temperature increase from 20℃ to 30℃ accelerated CDOM photobleaching more than it did to CDOM photoproduction.

Both the 20℃/10℃ and the 30℃/10℃ ratios of P_{DOC} in TPU (P_{DOC}-TPU) remained largely invariable throughout the irradiation period, with the day-7 rates at 20℃ and 30℃ being 125% and 413% higher than that at 10℃, respectively (Figure 11C). A similar constancy was also found for the ratios of P_{DN} in TPU; the day-7 rates at 20℃ and 30℃ surpassed that at 10℃ by 145% and 415%, respectively (Figure 11F). The 20℃/10℃ and 30℃/10℃ ratios of P_{CDOM} in TPU (P_{CDOM}-TPU) both declined during irradiation, slowly for the former and faster for the latter (Figure 11E). Temperature-dependence of CDOM photobleaching could have played a role if photobleaching of the TPU-derived CDOM led to little DOC loss (section 3.9). Despite the decreasing trends, P_{CDOM}-TPU was 256% higher at 20℃ than at 10℃ on day 4 and 200% on day 7, with the corresponding values for 30℃ *vs.*10℃ being 627% on day 4 and 414% on day 7.

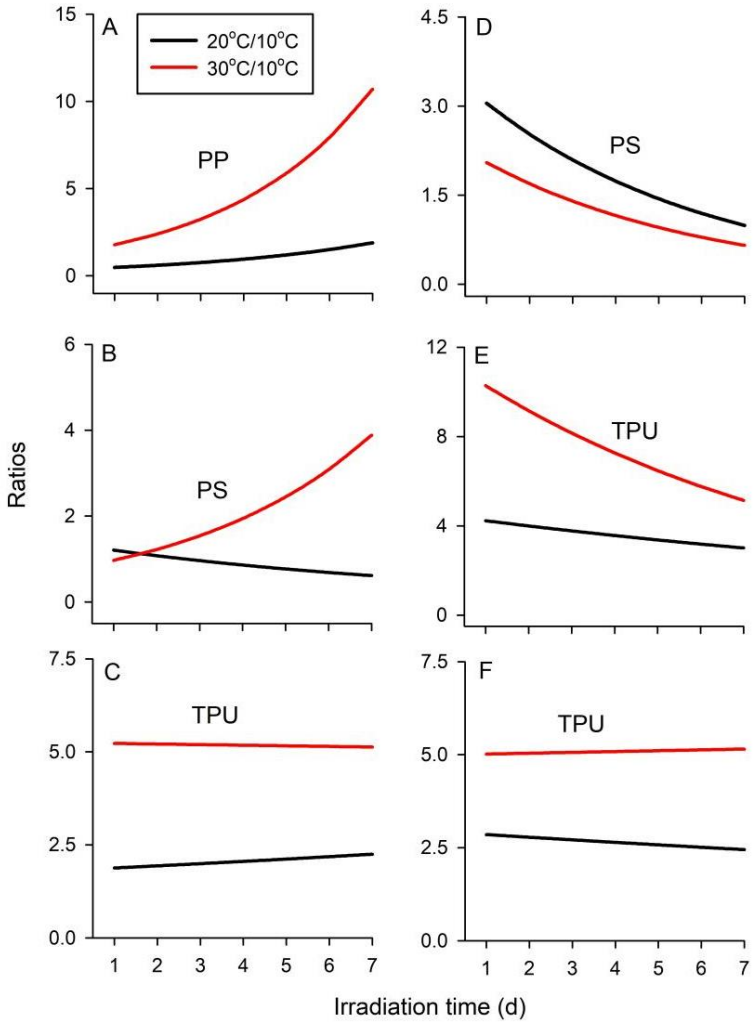

Figure 11: Ratios of photoproduction rates at 20℃ and 30℃ to that at 10℃. A-C: DOC; D and E: CDOM; F: DN.

Arrhenius plots were constructed to calculate the activation energies of DOM photoproduction from the MPs (Figure S4). The photoproduction rate (P; unit: μmol L^{-1} d^{-1} for DOC and DN and m^{-1} d^{-1} for CDOM) was fitted to temperature (T in Kelvins) using the equation:

$$\ln(P) = \ln(A) - E_a \times R^{-1} \times T^{-1} \qquad (1)$$

where A is a constant, E_a the activation energy (J mol^{-1}), and R the universal gas constant (8.314 J K^{-1} mol^{-1}). The activation energy for DOC photoproduction in PP on day 7 (84.8 kJ mol^{-1}) was 43% higher than that in TPU (59.4 kJ mol^{-1}) (Table 5), indicating a stronger temperature dependence of PP. The activation energies for DOC, CDOM, and DN photoproductions in TPU on day 7 were essentially identical (range: 57.0–59.4 kJ mol^{-1}). The activation energies for DOC and DN photoproductions in TPU remained rather constant while that for CDOM photoproduction decreased with irradiation time, as expected from the data shown in Figures. 11C,F,E (Table 5). The activation energy for photoproduction of CDOM in TPU on day 4 (70.8 kJ mol^{-1}) was 21% higher than that on day 7 (58.3 kJ mol^{-1}). Activation energies cannot be calculated for PS due to the "irregular" temperature-dependence behavior of the PS-derived DOM discussed earlier.

The positive temperature effect observed here suggests that diffusion-limited steps are involved in the photodissolution of MPs. This is in line with the view that secondary photoreactions involving free radicals play an important role in the degradation of plastics (Figure 3) (Andrady, 2011; Gewert et al., 2015). While direct photoreactions usually have very low activation energies, thermal reactions have much higher activation energies (Das and Tiwari, 2017). This may partly explain the higher activation energy for photoproduction of DOC in PP than that in TPU: TPU contains the chromophoric moieties that can directly absorb light and undergo degradation. The activation energies obtained here for MPs are considerably higher than those for photodegradation of natural DOM and POM (12–32 kJ mol^{-1}, mostly <20 kJ mol^{-1}) (Toole et al., 2003; Bouillon et al., 2006; Zhang et al., 2006; McKay et al., 2011; Estapa et al., 2012; Hong et al., 2014; Song

et al., 2017). Phase change during photodissolution of particles has been invoked to account for the higher activation energies for particulate matter than dissolved matter (Estapa et al., 2012). The highly ordered structures of synthetic plastics may further enhance the "cage" effect on the mobility of free radicals (Hartley and Guillet, 1968) and thus increase the activation energies of their photodissolution in comparison with natural organic matter.

The temperature effect on MPs photodegradation has been little explored. Ward et al. (2019) reported a 25% increase in the photooxidation of various formulations of PS with a 10°C increase in temperature in terms of photochemical oxygen consumption. This effect is much smaller than the 94% and 288% increases in P_{DOC}-PS in temperature observed in present study on days 4 and 7, respectively, for a 20°C increase in temperature. Note that our temperature effects are likely underestimated due to stronger photomineralization of the photoproduced DOC at 30°C *vs.* 10°C. Two factors could mainly contribute to this discrepancy. First, the photochemical oxygen consumption is a measure of the overall extent of oxidation of the plastics, which includes the partial photooxidation of the particulate form of the plastics, the photodissolution of the plastics into DOM, and the photomineralization of the plastics into CO_2. It could be that the temperature dependences of the partial photooxidation and photomineralization are weaker than that of the photodissolution. Second, the samples in the study of Ward et al. (2019) were exposed for up to 2 days, which is considerably shorter than the irradiation time of up to 7 days in the present study. As shown in Figure 11B, the temperature effect decreases exponentially with decreasing irradiation time. In fact, the temperature effect on P_{DOC}-PS for a 20°C increase was only 22% on day 2 in the present study. Although a direct comparison between the two studies is not possible due to the different experimental designs, our results call for attention to the importance of irradiation history in evaluating the temperature dependence of plastic photodegradation. A similar time-varying temperature dependence of photoalteration of the tensile extensibility of polypropylene plastics has been observed (Andrady, 2011).

Table 5: Fitted parameters for the Arrhenius equation describing the temperature dependences of photoproduction rates of DOC (P_{DOC}), DN (P_{DN}) and CDOM (P_{CDOM}, represented by a_{254}) (eq.1 in the main text). PP: polypropylene; TPU: thermoplastic polyurethane.

Microplastic	Time (day)	Ln(A)	Ea (kJ mol^{-1})	R^2	p
P_{DOC}					
PP	4	23.3 ± 13.4	52.47 ± 32.49	0.723	0.353
	7	38.2 ± 9.5	84.75 ± 23.23	0.930	0.170
TPU	4	27.8 ± 2.4	59.30 ± 5.79	0.991	0.062
	7	29.0 ± 0.9	59.39 ± 2.07	0.999	0.022
P_{CDOM}					
TPU	4	29.2 ± 4.1	70.75 ± 10.01	0.980	0.090
	7	25.4 ± 4.3	58.40 ± 10.36	0.970	0.112
P_{DN}					
TPU	4	24.3 ± 2.3	57.96 ± 5.64	0.991	0.062
	7	25.6 ± 0.8	57.99 ± 2.00	0.999	0.022

3.8. EFFECT OF LIGHT COMPOSITION

The accumulations of DOC under the UVA-plus-visible and visible-only treatments were marginal in PP and PS and insignificant in TPU compared to the dark controls (Figure 12), demonstrating that the observed photoproduction of DOC was essentially exclusively induced by UVB. The same was true for DN in TPU. This result supports the view that photooxidation of plastics in the marine environment is primarily initiated by solar UVB radiation (Andrady, 2011) and is consistent with the dominance of solar UVB over UVA and visible in initiating the photooxidation of PP in air (Zhang et al., 1996). However, studies probing the wavelength dependence of plastic photodegradation in aqueous media are rare. In a recent study, a visible light-absorbing additive (black rubber particles) was found to be able to promote photooxidation of PS at the wavelength of ~450 nm (Ward et al., 2019). Therefore, the wavelength dependence of plastic photooxidation relies on the chemical and optical properties of the additives contained in the plastics. This may have profound implications for plastic photooxidation in the water column, since visible light penetrates deeper than does UV radiation. Photooxidation of plastics which only absorb UVB radiation will thus be restricted to the thin UVB-penetrable layer, while photooxidation of those plastics which absorb both UV and visible light will take place down to greater depths, thereby increasing their oxidation rates.

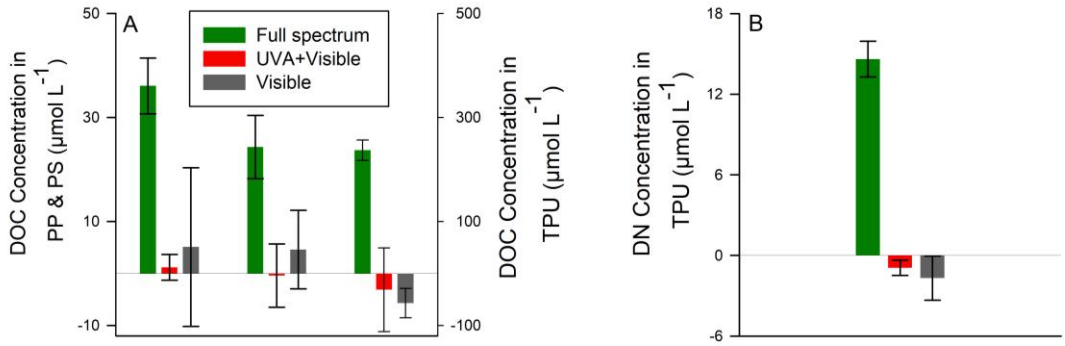

Figure 12: Accumulation of DOC in the PP, PS, TPU samples after 7 days of irradiation at 20°C under different light treatments. Dark controls have been subtracted from the light treatments. PP: polypropylene; PS: polystyrene; TPU: thermoplastic polyurethane.

3.9. PHOTODEGRADATION OF MP-DERIVED DOM

During the 14-d full-spectrum light exposure, the DOC produced from PP and TPU showed little loss (PP: 2%; TPU: 3%) (Figure 13A); the same was true for the DN from TPU (1%, Figure 13B). In contrast, the concentration of DOC derived from PS decreased with irradiation time, yielding a 13% and 16% (11.9 μmol L^{-1}) drawdown after 7 and 14 days of irradiation, respectively (Figure 13A). These results demonstrate that part of the PS-derived DOM was photomineralizable and that DOM collected from the post-irradiated PP and TPU samples appeared resistant to photodegradation. These results suggest that photooxidation of plastics can release photo-resistant DOC into the marine environment. Part of this DOC pool can be biolabile and thus fuel marine microbes, while the remaining component can be both photo- and bio-resistant and thus accumulate in the ocean (Romera-Castillo et al., 2018; L. Zhu et al., 2020).

The significant photodegradation of the PS-derived DOC indicates that the photoproduced DOC and CDOM measured in PS are underestimates. It is, however, difficult to quantitatively assess this underestimation, since the DOM collected from the post-irradiated MPs samples could have already been subjected to photodegradation during irradiation of the MPs. An underestimation of CDOM photoproduction from TPU is also possible, given that the possibility of CDOM photobleaching during the irradiation of this polymer cannot be ruled out (section 3.7).

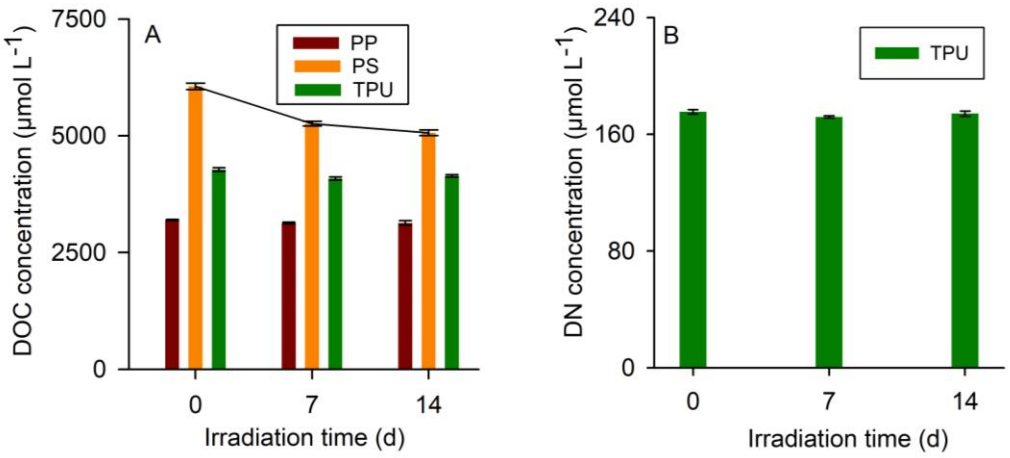

Figure 13: Photodegradability of dissolved organic carbon (A) and dissolved nitrogen (B) in filtrates (filter pore size: 0.2 µm) collected from microplastic samples that had been irradiated for 60 d at 30°C under full-spectrum simulated solar radiation. Dark controls have been subtracted from light treatments. PP: polypropylene; PS: polystyrene; TPU: thermoplastic polyurethane.

3.10. IMPLICATIONS FOR THE FATE OF MPs IN THE OCEAN

The lifetime (τ_{sea}, years) of a given type of MPs with respect to photodissolution at the sea surface was estimated using the following equation:

$$\tau_{sea} = [C_0 \times (P_{\mathrm{DOC}} \times V)^{-1}] \times (UVB_{\mathrm{lab}} \times UVB_{\mathrm{sea}}^{-1}) \times (0.80 \times 0.93 \times 365)^{-1} \quad (2)$$

where C_0 (μmol) stands for the initial carbon content in the MPs added to an irradiation cell; P_{DOC} (μmol L^{-1} d^{-1}) for the photoproduction rate of DOC in the irradiation cell; V (0.35 L) for the initial volume of the ASW medium in the irradiation cell; UVB_{lab} (mmol cm^{-2} d^{-1}) for the integrated UVB (290–320 nm) irradiance of the solar simulator; UVB_{sea} (mmol cm^{-2} d^{-1}) for the integrated UVB (290–320 nm) irradiance just above the sea surface; 0.80 and 0.93 are correction factors for the reflection of sunlight by cloud (Zafiriou et al., 2003) and water surface albedo (Zepp and Cline, 1977), respectively; 365 is a factor for converting days to years. C_0 was calculated by multiplying the percent carbon content (Table 2) by the initial amount of MPs added to the irradiation cell (147.0 mg). Clear-sky reference UVB_{sea} spectra were obtained from the study of Apell and McKneill (2019). The irradiance scaling factors, $UVB_{\mathrm{lab}}/UVB_{\mathrm{sea}}$, at latitudes of 0–60°N are shown in Table S2. The choice of UVB, instead of the entire UV or UV-visible regime, was based on the observation that photodissolution of the MPs tested was dominated by UVB (section 3.8). The range of 0–60°N was chosen for reference because it encompasses the 10 river mouths that export 90% of the plastic waster to the oceans (Schmidt et al., 2017; Ward et al., 2019). Two sets of P_{DOC} values were chosen: the linear rate on day 7 obtained from the 7-d time-series irradiation (i.e. [DOC] on day 7 divided by 7; all three temperatures tested) and the linear rate on day 60 obtained from the 60-d fixed-duration irradiation (i.e. [DOC] on day 60 divided by 60; 30°C only). In addition, the exponential model based on the 7-d irradiation (Figure 6, Table 4) was used to provide a third set of estimates, wherein τ_{sea} is derived as follows:

$$\tau_{\mathrm{sea}} = [b^{-1} \times \ln(a^{-1} \times C_0 \times V^{-1})] \times (UVB_{\mathrm{lab}} \times UVB_{\mathrm{sea}}^{-1}) \times (0.80 \times 0.93 \times 365)^{-1} \quad (3)$$

where *a* and *b* are fitted parameters for the exponential-rise equations for [DOC] (Table 4). The exponential model-derived lifetime serves as the lower limit, given that this model far overestimates the DOC production under the 60-d irradiation (section 3.4). The 60-d linear model is expected to give a lifetime closer to the real lifetime but the uncertainty involved is difficult to evaluate.

The lifetimes were calculated for the oceanic zones of 0–20°N (zone 1 hereinafter), 20–40°N (zone 2 hereinafter), and 40–60°N (zone 3 hereinafter), whose annual mean sea surface temperatures (27.5, 21.0, and 10.5°C, respectively, Bates et al., 1996) are close to the lab irradiation temperatures of 30°C, 20°C, and 10°C, respectively. As expected, the lifetimes of the MPs (Table 6) are shortest in zone 1, intermediate in zone 2, and longest in zone 3 due to a combination of the equatorward increases in solar irradiance and in water temperature. TPU showed the shortest lifetimes among the three types of polymers tested, irrespective of the geographic zone. The exponential model-based lifetimes are on the order of a few months and more than two orders of magnitude shorter than the 7-d linear model-based lifetimes for PP and PS and more than one order of magnitude shorter for TPU. The 60-d linear model yields lifetimes of a few years in zone 1, which are similar (for TPU) or one order of magnitude shorter (for PP and PS) than those based on the 7-d linear model. Notably, even the upper-bound lifetimes indicate that photodissolution can quickly remove TPU and be a significant sink for PP and PS in the surface ocean in all three zones. The shorter lifetimes in the warmer zones suggest that photodissolution could be a potentially important mechanism for explaining the missing sink of MPs in the subtropical ocean gyres (section 1.2.2. Cózar et al., 2014; Eriksen et al., 2014).

Table 6: Estimated lifetimes (units: years) of polypropylene (PP), polystyrene (PS), and thermoplastic polyurethane (TPU) in the oceanic zones of 0–20°N (zone 1), 20–40°N (zone 2), and 40–60°N (zone 3). The lower- and upper-bound lifetimes are based on the 7-day exponential and linear model for DOC photoproduction, respectively. Numbers in parentheses are based on the 60-d linear model for DOC photoproduction. Units: years

	0°–20°N	20°–40°N	40°–60°N
PP	0.17–13.4 (6.5)	0.28–87.8	0.69–171.4
PS	0.19–35.0 (3.6)	0.44–136.0	0.60–199.6
TPU	0.19–2.8 (3.7)	0.27–9.5	0.54–34.1

To evaluate the relative contributions of temperature and irradiance to the photodissolution of MPs at the surface ocean, we calculated the changes in lifetime when MPs are displaced from the warm zone 1 to the cold zone 3 under two scenarios: 1) the irradiance is kept at zone 1 while the temperature is decreased from zone 1 to zone 3 (i.e. 30°C→10°C); 2) the temperature is kept at zone 1 while irradiance is decreased from zone 1 to zone 3. The results indicate that scenario 1 (i.e. a 20°C decrease in temperature) increases the 7-d linear model-based lifetime ~3 times more than does scenario 2 (i.e. 2.3 times decrease in UVB irradiance) for PP and TPU but the difference between the two scenarios is marginal for PS (Table 7). Note that the temperature-dependence of PS photodissolution was underestimated due to the faster photochemical removal of the PS-derived DOC at higher temperatures (section 3.7), leading to a smaller effect of temperature on the lifetime of this polymer for scenario 1. This sensitivity analysis thus underscores the crucial role of temperature in controlling the persistence of MPs in cold water *vs.* in warm water with respect to photodissolution.

L. Zhu et al. (2020) determined photodegradation lifetimes of 0.3–4.3 years for PP MPs and 0.3–2.7 years for expanded PS MPs (irradiation temperature: 25–30°C) and Ward et al. (2019) obtained half-lives of 20–40 years (i.e. lifetimes: 29–58 years) for photooxidation of PS MPs with different formulations (irradiation temperature: 25°C). The lower limits of our 30°C-based lifetimes of PP (0.17 years) and PS (0.19 years) are similar to those by L. Zhu et al. (2020) that were also derived from an exponential-increase model for DOC photoproduction. It is, however, noteworthy that our lower limits could have been highly underestimated due to an unsustainable exponential DOC production under prolonged light exposure (section 3.4). Our 60-d linear model-based lifetimes for PP (6.5 years) and PS (3.6 years), which presumably better reflect the real lifetimes, generally agree with the upper-bound estimates by L. Zhu et al. (2020) derived from a linear extrapolation of microplastic mass loss over ~60 days of light exposure. The 7-d linear model-based lifetime for PS at 30°C in the present study (35.0 years) is within the range reported by Ward et al. (2019) who used an irradiation time of 5 days. The three studies thus give roughly comparable lifetimes under similar light exposure durations,

highlighting the importance of accounting for the light exposure history of MPs when comparing their photodegradation lifetimes from different studies. The differences remaining among the three studies (20–66%) could result from the use of different irradiation setups (MPs kept at the surface *vs.* well mixed in the irradiation cell) and of MPs with different formulations (virgin *vs.* postconsumer), shapes (pellets *vs.* films), and sizes (micrometers *vs.* millimeters).

The lifetimes estimated in this study involve potentially large uncertainties and thus only serve to provide preliminary information on the role of photodissolution in controlling the fate of MPs in the ocean. Aside from the time-varying photodissolution rate as discussed above, a few other variables could also produce sizable uncertainties for the estimated lifetimes. Positively buoyant MPs with sizes of sub-millimeters can be dispersed in the upper layer of the water column by turbulent mixing. A modeling study by Enders et al. (2015) has demonstrated that ~50% of the total microplastic particles of 100 μm is expected to be distributed in the top 25 m, with the remaining half located between 25 and 56 m. The microplastic samples under irradiation in our experiment were well mixed in the ASW with a thickness of 8–9 cm. As the penetration (e-folding) depth of the solar UVB radiation in the open ocean is usually <10 m (Yocis et al., 2000), the lifetimes estimated here are only applicable to MPs present in the top few meters in terms of the UVB depth distribution. Furthermore, PS (density: 1.05 g cm^{-3}) and TPU (density: 1.23 g cm^{-3}) are somewhat heavier than seawater (1.023 g cm^{-3} at salinity 35 and temperature 25°C). Hence, more PS and TPU particles are expected to be found in the deeper part of the surface layer and some of these particles may sink out of it. Biofouling of MPs can occur in the water column, which reduces the light available for plastic photodegradation. These three factors all lead to an underestimation of the lifetimes obtained in the present study. Several other factors could, however, overestimate the lifetimes. For example, the concentrations of MPs used in our study (420 mg L^{-1}; 72,694–652,477 particles L^{-1}) are two to three orders of magnitude higher than the maximum concentrations found in the surface ocean (359,748 particles m^{-3}, Chae et al., 2015). High concentrations of MPs could lead to self-shading, thereby reducing light absorption by

the MPs, although enhanced particle scattering may partially offset this effect. In addition, the accumulation of CDOM, particularly in TPU, during lab irradiation would also decrease the light available for plastic photodegradation. It is also worth noting that photodegradation of plastics produce not only DOC but also CO_2 (Ward et al., 2019; Tian et al., 2019) and volatile organic compounds (Royer et al., 2018). Although the CO_2 production is mostly minor compared to DOC production for PS (Ward et al., 2019), the relative contributions of these two pathways are unknown for other polymers.

Table 7: Change of photodissolution lifetimes (units: years) of microplastics at the ocean surface resulting from a displacement of the microplastic particles from zone 1 to zone 3 under two different scenarios: 1) irradiance is kept at zone 1 while water temperature is decreased to zone 3; 2) water temperature is kept at zone 1 while irradiance is deceased to zone 3 (see details in the text). Zone 1: 0°–20°N; zone 3: 40°–60°N. PP: polypropylene; PS: polystyrene; TPU: thermoplastic polyurethane.

	Temperature	Irradiance	PP	PS	TPU
Initial status	Zone 1	Zone 1	13.4	35.0	2.8
Senario 1	Zone 3	Zone 1	75.6	88.0	15.0
Senario 2	Zone 1	Zone 3	30.4	79.4	6.4
Senario 1/initial status			5.6	2.5	5.3
Senario 2/initial status			2.3	2.3	2.3

4. CONCLUSIONS AND PERSPECTIVES

This study quantified the photodissolution of three common types of MPs (PP, PS, and TPU) in artificial seawater in terms of photoproduction of DOC, CDOM, and DN; evaluated the effects of temperature and incident light composition on this photoprocess; and discussed the implications of photodissolution for the fate of these MPs in the surface ocean. Main conclusions from this study are summarized as follows:

1. TPU rapidly leaches out DOC and CDOM under dark conditions, likely from the additives contained in this polymer.

2. All three polymers produce DOC and CDOM photochemically; TPU produces DN as well. The production rates of these substances increase exponentially over an irradiation period of 7 days. Normalized to the initial plastic carbon present, PS and TPU are similarly efficient at producing DOC photochemically, while PP is about half as efficient as PS and TPU. Aliphatic ketones are likely among the chromophoric dissolved organic compounds produced photochemically by PP.

3. Photoproduction of DOC from all three polymers shows a stronger temperature-dependence than those of natural organic matter photoreactions. The temperature-dependence of DOC photoproduction from PP and PS increases with irradiation time, contrasting with the rather constant temperature-dependence of TPU photodissolution.

4. Photodissolution of all three polymers is almost entirely driven by UVB radiation, with little impact by UVA and visible radiation.

5. DOC photoproduced from PS is photomineralizable, while DOC photoproduced from PP and TPU appears to be photo-resistant.

6. The lifetime of TPU with respect to photodissolution at the ocean surface is estimated to be an order of magnitude shorter than those of PP and PS. The lifetimes in warm ocean waters are short enough for photodissolution to be an important mechanism for the missing sink of small MPs in the subtropical ocean gyres. Temperature is expected to play a more important role than is solar irradiance in controlling the photodissolution of these MPs when they move from warm waters to cold waters or vice versa.

It is challenging to evaluate the impact of photodegradation on the transport and fate of MPs accurately. First, the photodegradability of a given type of MPs depends on its size and shape and on the nature and content of the additives within it, all of which, particularly the size and shape, can vary considerably in natural environments, it is practically impossible to evaluate all these variables. Second, the effects of irradiation history of the MPs leads to large uncertainties in scaling up results based on short-term irradiation experiments. Lengthy, resource-costly tests that ideally lead to complete photodissolution are needed to capture the full pictures of the effect of the light exposure history. Third, although MPs that are smaller than 1 mm tend to be afloat at the sea surface, sub-millimeter-sized MPs can be dispersed by turbulence into the subsurface (Enders et al., 2015) where UV radiation is weaker or even absent. To simulate *in situ* mixing processes is tricky and often requires sophisticated and expensive experimental setup. Alternatively, coupled physical-optical-photochemical models, similar to those implemented for studying CDOM photochemistry (Sikorski and Zika, 1993a, 1993b; Doney et al., 1995; Von Hobe et al., 2003), need to be developed to address this issue. Fourth, biofouling of MPs not only reduces the light available for plastic photodegradation but also tends to increase the density of the MPs (Kaiser et al., 2017; Kooi et al., 2017) and thus reduce their residence time in the sunlit surface layer. As the extent of biofouling and the biofilm composition vary with time (Kaiser et al., 2017), incorporating the biofouling effect into photochemical studies of MPs remains a major challenge. Finally, plastic photodegradation generates three classes of carbon products: DOC, CO_2, and volatile organic compounds. To our knowledge, these products have not been measured simultaneously in a single study, probably due in part to the demanding

requirements for the design of irradiation experiments, as well as for analytical resources. However, to better assess the overall photodegradation rate of MPs, future studies should strive to quantify these products collectively, along with a concomitant measurement of the changes in the mass and elemental composition of the MPs.

BIBLIOGRAPHY

Alimba, C.G., Faggio, C., 2019. Microplastics in the marine environment: Current trends in environmental pollution and mechanisms of toxicological profile. Environ. Toxicol. Pharmacol. 68, 61–74. https://doi.org/10.1016/j.etap.2019.03.001

Andrady, A.L., 2011. Microplastics in the marine environment. Mar. Pollut. Bull. 62, 1596–1605. https://doi.org/10.1016/j.marpolbul.2011.05.030

Andrady, A.L., 2015. Degradation of Plastics in the Environment. In: Plastics and environmental sustainability. Wiley, Hoboken, pp. 145–184. https://doi.org/10.1002/9781119009405.ch6

Apell, J.N., McNeill, K., 2019. Updated and validated solar irradiance reference spectra for estimating environmental photodegradation rates. Environ. Sci. Process. Impacts 21, 427–437. https://doi.org/10.1039/c8em00478a

Arthur, C., Baker, J., Bamford, H., 2009. Proceedings of the International Research Workshop on the Occurrence , Effects , and Fate of Microplastic Marine Debris. Group 530.

Au, S.Y., Bruce, T.F., Bridges, W.C., Klaine, S.J., 2015. Responses of Hyalella azteca to acute and chronic microplastic exposures. Environ. Toxicol. Chem. 34, 2564–2572. https://doi.org/10.1002/etc.3093

Auta, H.S., Emenike, C.U., Fauziah, S.H., 2017. Distribution and importance of microplastics in the marine environmentA review of the sources, fate, effects, and potential solutions. Environ. Int. 102, 165–176. https://doi.org/10.1016/j.envint.2017.02.013

Babin, M., Stramski, D., Ferrari, G.M., Claustre, H., Bricaud, A., Obolensky, G., Hoepffner, N., 2003. Variations in the light absorption coefficients of phytoplankton, nonalgal particles, and dissolved organic matter in coastal waters around Europe. J. Geophys. Res. Ocean. 108. https://doi.org/10.1029/2001jc000882

°CBarrón, C., Duarte, C.M., 2015. Dissolved organic carbon pools and export from the coastal ocean. Global Biogeochem. Cycles 29, 1725–1738. https://doi.org/10.1002/2014GB005056.

Bascom, W., 1974. The Disposal of Waste in the Ocean. Sci. Am. 231, 16–25. https://doi.org/10.1038/scientificamerican0874-16

Bates, T.S., Kelly, K.C., Johnson, J.E., Gammon, R.H., 1996. A reevaluation of the open ocean source of methane to the atmosphere. J. Geophys. Res.: Atmos. 101, 6953–6961. https://doi.org/10.1029/95JD03348

Belzile, C., Brugel, S., Nozais, C., Gratton, Y., Demers, S., 2008. Variations of the abundance and nucleic acid content of heterotrophic bacteria in Beaufort Shelf waters during winter and spring. J. Mar. Syst. 74, 946–956. https://doi.org/10.1016/j.jmarsys.2007.12.010

Blough, N.V., Zepp, R.G., 1995. Reactive oxygen species in natural waters. In: Foote, C.S., Valentine, J., Greenberg, A., Liebman, J.F. (Eds.), Active oxygen in chemistry. Structure Energetics and Reactivity in Chemistry Series (SEARCH Series), vol 2. Springer, Dordrecht, pp. 280–333. https://doi.org/10.1007/978-94-007-0874-7_8

Boucher, J., Friot, D., 2017. Primary microplastics in the oceans: A global evaluation of sources, Primary microplastics in the oceans: A global evaluation of sources. https://doi.org/10.2305/iucn.ch.2017.01.en

Bouillon, R.C., Knierim, T.L., Kieber, R.J., Skrabal, S.A., Wright, J.L.C., 2006. Photodegradation of the algal toxin domoic acid in natural water matrices. Limnol. Oceanogr. 51, 321–330. https://doi.org/10.4319/lo.2006.51.1.0321

Browne, M.A., Niven, S.J., Galloway, T.S., Rowland, S.J., Thompson, R.C., 2013. Microplastic moves pollutants and additives to worms, reducing functions linked to health and biodiversity. Curr. Biol. 23, 2388–2392. https://doi.org/10.1016/j.cub.2013.10.012

Bushaw, K.L., Zepp, R.G., Tarr, M.A., Schulz-Jander, D., Bourbonniere, R.A., Hodson, R.E., Miller, W.L., Bronk, D.A., Moran, M.A., 1996. Photochemical release of biologically available nitrogen from aquatic dissolved organic matter. Nature, 381, 404–407. https://doi.org/10.1038/381404a0

Caron, A.G.M., Thomas, C.R., Berry, K.L.E., Motti, C.A., Ariel, E., Brodie, J.E., 2018. Ingestion of microplastic debris by green sea turtles (Chelonia mydas) in the Great Barrier Reef: Validation of a sequential extraction protocol. Mar. Pollut. Bull. 127, 743–751. https://doi.org/10.1016/j.marpolbul.2017.12.062

Chae, D.H., Kim, I.S., Kim, S.K., Song, Y.K., Shim, W.J., 2015. Abundance and Distribution Characteristics of Microplastics in Surface Seawaters of the Incheon/Kyeonggi Coastal Region. Arch. Environ. Contam. Toxicol. 69, 269–278. https://doi.org/10.1007/s00244-015-0173-4

Chen, P.J., Linden, K.G., Hinton, D.E., Kashiwada, S., Rosenfeldt, E.J., Kullman, S.W., 2006. Biological assessment of bisphenol A degradation in water following direct photolysis and UV advanced oxidation. Chemosphere 65, 1094–1102. https://doi.org/10.1016/j.chemosphere.2006.04.048

Cincinelli, A., Scopetani, C., Chelazzi, D., Lombardini, E., Martellini, T., Katsoyiannis, A., Fossi, M.C., Corsolini, S., 2017. Microplastic in the surface waters of the Ross Sea (Antarctica): Occurrence, distribution and characterization by FTIR. Chemosphere 175, 391–400. https://doi.org/10.1016/j.chemosphere.2017.02.024

Clark, C.D., Zika, R.G., 2000. Marine organic photochemistry: from the sea surface to marine aerosols. In: Wangersky, P.J. (Ed.), Marine chemistry. Springer, Berlin, Heidelberg, pp. 1–33. https://doi.org/10.1007/10683826_1

Cole, M., Lindeque, P., Halsband, C., Galloway, T.S., 2011. Microplastics as contaminants in the marine environment: A review. Mar. Pollut. Bull. 62, 2588–2597. https://doi.org/10.1016/j.marpolbul.2011.09.025

Collignon, A., Hecq, J.H., Glagani, F., Voisin, P., Collard, F., Goffart, A., 2012. Neustonic microplastic and zooplankton in the North Western Mediterranean Sea. Mar. Pollut. Bull. 64, 861–864. https://doi.org/10.1016/j.marpolbul.2012.01.011

Colton, J.., Knapp, F.., Burns, B.., 1974. Plastic particles in surface waters of the northwestern Atlantic. Science, 185, 491–497. https://doi.org/10.1126/science.185.4150.491

Cooper, W. J., Herr, F. L., 1987. Introduction and overview. In: Zika, R. G., Cooper, W. J. (Eds.), Photochemistry of environmental aquatic systems. ACS Symposium Series; American Chemical Society: Washington, DC, pp. 1–6. https://doi.org/10.1021/bk-1987-0327.ch001

Cózar, A., Echevarría, F., González-Gordillo, J.I., Irigoien, X., Úbeda, B., Hernández-León, S., Palma, Á.T., Navarro, S., García-de-Lomas, J., Ruiz, A., Fernández-de-Puelles, M.L., Duarte, C.M., 2014. Plastic debris in the open ocean. Proc. Natl. Acad. Sci. U. S. A. 111, 10239–10244. https://doi.org/10.1073/pnas.1314705111

Cózar, A., Sanz-Martín, M., Martí, E., González-Gordillo, J.I., Ubeda, B., Á.gálvez, J., Irigoien, X., Duarte, C.M., 2015. Plastic accumulation in the mediterranean sea. PLoS One 10, 1–12. https://doi.org/10.1371/journal.pone.0121762

Crawford, C. B., Quinn, B., 2016. Physiochemical properties and degradation. In: Microplastic pollutants, 1st ed. Elsevier Limited, pp. 89–94. https://doi.org/10.1016/B978-0-12-809406-8.00004-9

Das, P., Tiwari, P., 2017. Thermal degradation kinetics of plastics and model selection. Thermochim. Acta 654, 191–202. https://doi.org/10.1016/j.tca.2017.06.001

de Lucia, G.A., Caliani, I., Marra, S., Camedda, A., Coppa, S., Alcaro, L., Campani, T., Giannetti, M., Coppola, D., Cicero, A.M., Panti, C., Baini, M., Guerranti, C., Marsili, L., Massaro, G., Fossi, M.C., Matiddi, M., 2014. Amount and distribution of neustonic micro-plastic off the western Sardinian coast (Central-Western Mediterranean Sea). Mar. Environ. Res. 100, 10–16. https://doi.org/10.1016/j.marenvres.2014.03.017

Desforges, J.P.W., Galbraith, M., Dangerfield, N., Ross, P.S., 2014. Widespread distribution of microplastics in subsurface seawater in the NE Pacific Ocean. Mar. Pollut. Bull. 79, 94–99. https://doi.org/10.1016/j.marpolbul.2013.12.035

Desforges, J.P.W., Galbraith, M., Ross, P.S., 2015. Ingestion of Microplastics by Zooplankton in the Northeast Pacific Ocean. Arch. Environ. Contam. Toxicol. 69. https://doi.org/10.1007/s00244-015-0172-5

Doney, S.C., Najjar, R.G., Stewart, S., 1995. Photochemistry, mixing and diurnal cycles in the upper ocean. J. Mar. Res. 53, 341–369. https://doi.org/10.1357/0022240953213133

Dong, D., Tasaka, S., Aikawa, S., Kamiya, S., Inagaki, N., Inoue, Y., 2001. Thermal degradation of acrylonitrile–butadiene–styrene terpolymer in bean oil. Polym. Degrad. Stab., 73, 319-326. https://doi.org/10.1016/S0141-3910(01)00093-3

Duis, K., Coors, A., 2016. Microplastics in the aquatic and terrestrial environment: sources (with a specific focus on personal care products), fate and effects. Environ. Sci. Eur. 28, 1–25. https://doi.org/10.1186/s12302-015-0069-y

Enders, K., Lenz, R., Stedmon, C.A., Nielsen, T.G., 2015. Abundance, size and polymer composition of marine microplastics ≥10 μm in the Atlantic Ocean and their modelled vertical distribution. Mar. Pollut. Bull. 100, 70–81. https://doi.org/10.1016/j.marpolbul.2015.09.027

Eriksen, M., Lebreton, L.C.M., Carson, H.S., Thiel, M., Moore, C.J., Borerro, J.C., Galgani, F., Ryan, P.G., Reisser, J., 2014. Plastic Pollution in the World's Oceans: More than 5 Trillion Plastic Pieces Weighing over 250,000 Tons Afloat at Sea. PLoS One 9, 1–15. https://doi.org/10.1371/journal.pone.0111913

Eriksen, M., Maximenko, N., Thiel, M., Cummins, A., Lattin, G., Wilson, S., Hafner, J., Zellers, A., Rifman, S., 2013. Plastic pollution in the South Pacific subtropical gyre. Mar. Pollut. Bull. 68, 71–76. https://doi.org/10.1016/j.marpolbul.2012.12.021

Estapa, M.L., Mayer, L.M., 2010. Photooxidation of particulate organic matter, carbon/oxygen stoichiometry, and related photoreactions. Mar. Chem. 122, 138–147. https://doi.org/10.1016/j.marchem.2010.06.003

Estapa, M.L., Mayer, L.M., Boss, E., 2012. Rate and apparent quantum yield of photodissolution of sedimentary organic matter. Limnol. Oceanogr. 57, 1743–1756. https://doi.org/10.4319/lo.2012.57.6.1743

Farrell, P., Nelson, K., 2013. Trophic level transfer of microplastic: Mytilus edulis (L.) to Carcinus maenas (L.). Environ. Pollut. 177, 1–3. https://doi.org/10.1016/j.envpol.2013.01.046

Galí, M., Kieber, D.J., Romera-Castillo, C., Kinsey, J.D., Devred, E., Pérez, G.L., Westby, G.R., Marrasé, C., Babin, M., Levasseur, M., Duarte, C.M., Agustí, S., Simó, R., 2016. CDOM sources and photobleaching control quantum yields for oceanic DMS photolysis. Environ. Sci. Technol. 50, 13361–13370. https://doi.org/10.1021/acs.est.6b04278

Galloway, T.S., Lee, B.P., Burić, I., Steele, A.M., Kocur, A.L., Pandeth, A.G., Harries, L.W., 2019. Plastics Additives and Human Health: A Case Study of Bisphenol A (BPA). Issues Environ. Sci. Technol. 2019-Janua, 131–155. https://doi.org/10.1039/9781788013314-00131

Gewert, B., Plassmann, M.M., Macleod, M., 2015. Pathways for degradation of plastic polymers floating in the marine environment. Environ. Sci. Process. Impacts 17, 1513–1521. https://doi.org/10.1039/c5em00207a

Geyer, R., Jambeck, J.R., Law, K.L., 2017. Production, use, and fate of all plastics ever made. Sci. Adv. 3, 25–29. https://doi.org/10.1126/sciadv.1700782

Goldstein, M.C., Titmus, A.J., Ford, M., 2013. Scales of spatial heterogeneity of plastic marine debris in the northeast Pacific Ocean. PLoS One 8. https://doi.org/10.1371/journal.pone.0080020

Gündoğdu, S., 2017. High level of micro-plastic pollution in the Iskenderun Bay NE Levantine coast of Turkey. Ege J. Fish. Aquat. Sci. 34, 401–408. https://doi.org/10.12714/egejfas.2017.34.4.06

Hahladakis, J.N., Velis, C.A., Weber, R., Iacovidou, E., Purnell, P., 2018. An overview of chemical additives present in plastics: Migration, release, fate and environmental impact during their use, disposal and recycling. J. Hazard. Mater. 344, 179–199. https://doi.org/10.1016/j.jhazmat.2017.10.014

Hale, R.C., Seeley, M.E., La Guardia, M.J., Mai, L., Zeng, E.Y., 2020. A Global Perspective on Microplastics. J. Geophys. Res. Ocean. 125, 1–40. https://doi.org/10.1029/2018JC014719

Hartley, G.H., Guillet, J.E., 1968. Photochemistry of ketone polymers. I. Studies of ethylene-carbon monoxide copolymers. Macromolecules. 1, 165–170. https://doi.org/10.1021/ma60002a012

Hefner, K.H., Fisher, J.M., Ferry, J.L., 2006. A multifactor exploration of the photobleaching of Suwannee River dissolved organic matter across the freshwater/saltwater interface. Environ. Sci. Technol. 40, 3717–3722. https://doi.org/10.1021/es052513h

Hélie, J.-F., 2009. Elemental and stable isotopic approaches for studying the organic and inorganic carbon components in natural samples. IOP Conf. Ser. Earth Environ. Sci. 5, 012005. https://doi.org/10.1088/1755-1307/5/1/012005

Hong, J., Xie, H., Guo, L., Song, G., 2014. Carbon monoxide photoproduction: Implications for photoreactivity of arctic permafrost-derived soil dissolved organic matter. Environ. Sci. Technol. 48, 9113–9121. https://doi.org/10.1021/es502057n

Isobe, A., Uchida, K., Tokai, T., Iwasaki, S., 2015. East Asian seas: A hot spot of pelagic microplastics. Mar. Pollut. Bull. 101, 618–623. https://doi.org/10.1016/j.marpolbul.2015.10.042

Jacobs, L.E., Weavers, L.K., Chin, Y.P., 2008. Direct and indirect photolysis of polycyclic aromatic hydrocarbons in nitrate-rich surface waters. Environ. Toxicol. Chem. 27, 1643–1648. https://doi.org/10.1897/07-478.1

Jambeck, J.R., Geyer, R., Wilcox, C., Siegler, T.R., Perryman, M., Andrady, A., Narayan, R., Law, K.L., 2015. Plastic waste inputs from land into the ocean. Science, 347, 768–771. https://doi.org/10.1126/science.1260352

Jasso-Gastinel, C.F., Soltero-Martínez, J.F.A., Mendizábal, E., 2017. Introduction: modifiable characteristics and applications. In: Jasso-Gastinel,C.F., Kenny, J.M. (Eds.), Modification of polymer properties, 1st ed. William Andrew Publishing, pp. 1–21. https://doi.org/10.1016/B978-0-323-44353-1.00001-4

Johannessen, S.C., Miller, W.L., 2001. Quantum yield for the photochemical production of dissolved inorganic carbon in seawater. Mar. Chem. 76, 271–283. https://doi.org/10.1016/S0304-4203(01)00067-6

Kaiser, D., Kowalski, N., Waniek, J.J., 2017. Effects of biofouling on the sinking behavior of microplastics. Environ. Res. Lett. 12, p. 124003. https://doi.org/10.1088/1748-9326/aa8e8b

Kalsi, P.S., 2007. Ultraviolet (UV) and visible spectroscopy. In: Spectroscopy of organic compounds, 6th ed. New age international. pp. 9–22.

Kang, J.H., Kwon, O.Y., Lee, K.W., Song, Y.K., Shim, W.J., 2015. Marine neustonic microplastics around the southeastern coast of Korea. Mar. Pollut. Bull. 96, 304–312. https://doi.org/10.1016/j.marpolbul.2015.04.054

Kaplan, L.A., Cory, R.M., 2016. Dissolved organic matter in stream ecosystems: forms, functions, and fluxes of watershed Tea. In: Jones, J.B., Stanley, E. (Eds), Stream ecosystems in a changing environment. Academic Press, pp. 241–320. https://doi.org/10.1016/B978-0-12-405890-3.00006-3

Katagi, T., 2018. Direct photolysis mechanism of pesticides in water. J. Pestic. Sci. 43, 57–72. https://doi.org/10.1584/jpestics.D17-081

Kershaw, P., Katsuhiko, S., Lee, S., Woodring, D., 2011. Plastic debris in the ocean. United Nations Environment Programme. pp. 20–26.

Kieber, R.J., Li, A., Seaton, P.J., 1999. Production of nitrite from the photodegradation of dissolved organic matter in natural waters. Environ. Sci. Technol. 33, 993–998. https://doi.org/10.1021/es980188a

Kieber, R.J., Whitehead, R.F., Skrabal, S.A., 2006. Photochemical production of dissolved organic carbon from resuspended sediments. Limnol. Oceanogr. 51, 2187–2195. https://doi.org/10.4319/lo.2006.51.5.2187

Kikugawa, K., Beppu, M., 1987. Involvement of lipid oxidation products in the formation of fluorescent and cross-linked proteins. Chem. Phys. Lipids. 44, 277–296. https://doi.org/10.1016/0009-3084(87)90054-5

Klein, S., Dimzon, I.K., Eubeler, J., Knepper, T.P., 2018. Analysis, occurrence, and degradation of microplastics in the aqueous environment. In: Wagner, M., Lambert, S. (Eds.), Freshwater microplastics, The Handbook of Environmental Chemistry, vol 58. Springer, Cham, pp. 51–67. https://doi.org/10.1007/978-3-319-61615-5_3

Kooi, M., Nes, E.H.V., Scheffer, M., Koelmans, A.A., 2017. Ups and downs in the ocean: effects of biofouling on vertical transport of microplastics. Environ. Sci. Technol. 51, 7963–7971. https://doi.org/10.1021/acs.est.6b04702

Lacoste, J., Vaillant, D., Carlsson, D.J., 1993. Gamma-, photo-, and thermally-initiated oxidation of isotactic polypropylene. J. Polym. Sci., Part A: Polym. Chem. 31, 715–722. https://doi.org/10.1002/pola.1993.080310316

Lambert, S., Wagner, M., 2016. Characterisation of nanoplastics during the degradation of polystyrene. Chemosphere 145, 265–268. https://doi.org/10.1016/j.chemosphere.2015.11.078

Laudon, H., Köhler, S., Buffam, I., 2004. Seasonal TOC export from seven boreal catchments in northern Sweden. Aquat. Sci. 66, 223–230. https://doi.org/10.1007/s00027-004-0700-2

Lavender Law, K., Morét-Ferguson, S., Maximenko, N.A., Peacock, E.E., Hafner, J., Reddy, C.M., 2010. Plastic Accumulation in the North Atlantic Subtropical Gyre Published by : American Association for the Advancement of Science Linked references are available on JSTOR for this article : Plastic Accumulation in the North Atlantic Subtropical Gyre 329, 1185–1188.

Law, K.L., Morét-Ferguson, S.E., Goodwin, D.S., Zettler, E.R., Deforce, E., Kukulka, T., Proskurowski, G., 2014. Distribution of surface plastic debris in the eastern pacific ocean from an 11-year data set. Environ. Sci. Technol. 48, 4732–4738. https://doi.org/10.1021/es4053076

Law, K.L., Thompson, R.C., 2014. Microplastics in the seas. Science (80-.). 345, 144–145. https://doi.org/10.1126/science.1254065

Lebreton, L., Slat, B., Ferrari, F., Sainte-Rose, B., Aitken, J., Marthouse, R., Hajbane, S., Cunsolo, S., Schwarz, A., Levivier, A., Noble, K., Debeljak, P., Maral, H., Schoeneich-Argent, R., Brambini, R., Reisser, J., 2018. Evidence that the Great Pacific Garbage Patch is rapidly accumulating plastic. Sci. Rep. 8, 1–15. https://doi.org/10.1038/s41598-018-22939-w

Lee, K.W., Shim, W.J., Kwon, O.Y., Kang, J.H., 2013. Size-dependent effects of micro polystyrene particles in the marine copepod tigriopus japonicus. Environ. Sci. Technol. 47, 11278–11283. https://doi.org/10.1021/es401932b

Lönnstedt, O.M., Eklöv, P., 2016. Environmentally relevant concentrations of microplastic particles influence larval fish ecology. Science (80-.). 352, 1213–1216. https://doi.org/10.1126/science.aad8828

Lorenz, C., Roscher, L., Meyer, M.S., Hildebrandt, L., Prume, J., Löder, M.G.J., Primpke, S., Gerdts, G., 2019. Spatial distribution of microplastics in sediments and surface waters of the southern North Sea. Environ. Pollut. 252, 1719–1729. https://doi.org/10.1016/j.envpol.2019.06.093

Lusher, A.L., Burke, A., O'Connor, I., Officer, R., 2014. Microplastic pollution in the Northeast Atlantic Ocean: Validated and opportunistic sampling. Mar. Pollut. Bull. 88, 325–333. https://doi.org/10.1016/j.marpolbul.2014.08.023

Lusher, A.L., Tirelli, V., O'Connor, I., Officer, R., 2015. Microplastics in Arctic polar waters: The first reported values of particles in surface and sub-surface samples. Sci. Rep. 5, 1–10. https://doi.org/10.1038/srep14947

Mayer, L.M., Schick, L.L., Bianchi, T.S., Wysocki, L.A., 2009a. Photochemical changes in chemical markers of sedimentary organic matter source and age. Mar. Chem. 113, 123–128. https://doi.org/10.1016/j.marchem.2009.01.006

Mayer, L.M., Schick, L.L., Hardy, K.R., Estapa, M.L., 2009b. Photodissolution and other photochemical changes upon irradiation of algal detritus. Limnol. Oceanogr. 54, 1688–1698. https://doi.org/10.4319/lo.2009.54.5.1688

Mayer, L.M., Schick, L.L., Skorko, K., Boss, E., 2006. Photodissolution of particulate organic matter from sediments. Limnol. Oceanogr. 51, 1064–1071. https://doi.org/10.4319/lo.2006.51.2.1064

McKay, G., Dong, M.M., Kleinman, J.L., Mezyk, S.P., Rosario-Ortiz, F.L., 2011. Temperature dependence of the reaction between the hydroxyl radical and organic matter. Environ. Sci. Technol. 45, 6932–6937. https://doi.org/10.1021/es201363j

Miller, W.L., Zepp, R.G., 1995. Photochemical production of dissolved inorganic carbon from terrestrial organic matter: Significance to the oceanic organic carbon cycle. Geophys. Res. Lett. 22, 417–420. https://doi.org/10.1029/94GL03344

Min, K., Cuiffi, J.D., Mathers, R.T., 2020. Ranking environmental degradation trends of plastic marine debris based on physical properties and molecular structure. Nat. Commun. 11. https://doi.org/10.1038/s41467-020-14538-z

Moore, C.J., Moore, S.L., Leecaster, M.K., Weisberg, S.B., 2001. A comparison of plastic and plankton in the North Pacific Central Gyre. Mar. Pollut. Bull. 42, 1297–1300. https://doi.org/10.1016/S0025-326X(01)00114-X

Mopper, K., Kieber, D.J., Stubbins, A., 2015. Marine photochemistry of organic matter: processes and impacts. In: Hansell, D.A., Carlson, C.A. (Eds), Biogeochemistry of marine dissolved organic matter, 2nd ed. Academic Press, pp. 422–425. https://doi.org/10.1016/B978-0-12-405940-5.00008-X

Moran, M.A., Zepp, R.G., 1997. Role of photoreactions in the formation of biologically labile compounds from dissolved organic matter. Limnol. Oceanogr. 42, 1307–1316. https://doi.org/10.4319/lo.1997.42.6.1307

Morgana, S., Ghigliotti, L., Estévez-Calvar, N., Stifanese, R., Wieckzorek, A., Doyle, T., Christiansen, J.S., Faimali, M., Garaventa, F., 2018. Microplastics in the Arctic: A case study with sub-surface water and fish samples off Northeast Greenland. Environ. Pollut. 242, 1078–1086. https://doi.org/10.1016/j.envpol.2018.08.001

Nelms, S.E., Galloway, T.S., Godley, B.J., Jarvis, D.S., Lindeque, P.K., 2018. Investigating microplastic trophic transfer in marine top predators. Environ. Pollut. 238, 999–1007. https://doi.org/10.1016/j.envpol.2018.02.016

Neves, D., Sobral, P., Ferreira, J.L., Pereira, T., 2015. Ingestion of microplastics by commercial fish off the Portuguese coast. Mar. Pollut. Bull. 101, 119–126. https://doi.org/10.1016/j.marpolbul.2015.11.008

Padsalgikar, A., 2017. Biological properties of plastics. In: Plastics in medical devices for cardiovascular applications. United Kingdom: Elsevier Science, pp. 92–93. https://doi.org/10.1016/B978-0-323-35885-9.00004-7

Pan, Z., Liu, Q., Sun, Y., Sun, X., Lin, H., 2019. Environmental implications of microplastic pollution in the Northwestern Pacific Ocean. Mar. Pollut. Bull. 146, 215–224. https://doi.org/10.1016/j.marpolbul.2019.06.031

Pelizzetti, E., Calza, P., 2002. Photochemical processes in the euphotic zone of sea water: Progress and problems. In: Chemistry of marine water and sediments, Gianguzza, A., Pelizzetti, E., Sammartano, S. (Eds.). Springer, Berlin, Heidelberg, pp. 83–103. https://doi.org/10.1007/978-3-662-04935-8_3

Pisani, O., Yamashita, Y., Jaffé Rudolf, R., 2011. Photo-dissolution of flocculent, detrital material in aquatic environments: Contributions to the dissolved organic matter pool. Water Res. 45, 3836–3844. https://doi.org/10.1016/j.watres.2011.04.035

Pivokonsky, M., Cermakova, L., Novotna, K., Peer, P., Cajthaml, T., Janda, V., 2018. Occurrence of microplastics in raw and treated drinking water. Sci. Total Environ. 643, 1644–1651. https://doi.org/10.1016/j.scitotenv.2018.08.102

PlasticsEurope., 2020. Plastics-the Facts 2020 An analysis of european plastics production, demand and waste data. Retrieved from https://www.plasticseurope.org/en/resources/publications/4312-plastics-facts-2020

Polymer Properties Database., 2015. Retrieved from https://polymerdatabase.com/polymer%20chemistry/Hydrolysis.html

Pospíšil, J., Nešpůrek, S., 1997. Highlights in chemistry and physics of polymer stabilization. Macromol. Symp. 115, 143–163. https://doi.org/10.1002/masy.19971150110

Provencher, J.F., Vermaire, J.C., Avery-Gomm, S., Braune, B.M., Mallory, M.L., 2018. Garbage in guano? Microplastic debris found in faecal precursors of seabirds known to ingest plastics. Sci. Total Environ. 644, 1477–1484. https://doi.org/10.1016/j.scitotenv.2018.07.101

Reisser, J., Slat, B., Noble, K., Du Plessis, K., Epp, M., Proietti, M., De Sonneville, J., Becker, T., Pattiaratchi, C., 2015. The vertical distribution of buoyant plastics at sea: An observational study in the North Atlantic Gyre. Biogeosciences 12, 1249–1256. https://doi.org/10.5194/bg-12-1249-2015

Riggsbee, J.A., Orr, C.H., Leech, D.M., Doyle, M.W., Wetzel, R.G., 2008. Suspended sediments in river ecosystems: Photochemical sources of dissolved organic carbon, dissolved organic nitrogen, and adsorptive removal of dissolved iron. J. Geophys. Res. Biogeosciences 113, 1–12. https://doi.org/10.1029/2007JG000654

Riley, G.A., 1971. Particulate organic matter in sea water. In: Russell, F.S, Yonge, M. (Eds.), Advances in marine biology. Academic Press, Volume 8, pp. 1–118. https://doi.org/10.1016/S0065-2881(08)60491-5

Rist, S.E., Assidqi, K., Zamani, N.P., Appel, D., Perschke, M., Huhn, M., Lenz, M., 2016. Suspended micro-sized PVC particles impair the performance and

decrease survival in the Asian green mussel Perna viridis. Mar. Pollut. Bull. 111, 213–220. https://doi.org/10.1016/j.marpolbul.2016.07.006

Rochman, C.M., Kurobe, T., Flores, I., Teh, S.J., 2014. Early warning signs of endocrine disruption in adult fish from the ingestion of polyethylene with and without sorbed chemical pollutants from the marine environment. Sci. Total Environ. 493, 656–661. https://doi.org/10.1016/j.scitotenv.2014.06.051

Rohatgi-Mukherjee, K. K., 1978. Introducing photochemistry. In: Fundamentals of photochemistry, 2nd ed. New Age International, pp. 1–9.

Romera-Castillo, C., Pinto, M., Langer, T.M., Álvarez-Salgado, X.A., Herndl, G.J., 2018. Dissolved organic carbon leaching from plastics stimulates microbial activity in the ocean. Nat. Commun. 9. https://doi.org/10.1038/s41467-018-03798-5

Rosu, D., Rosu, L., Cascaval, C.N., 2009. IR-change and yellowing of polyurethane as a result of UV irradiation. Polym. Degrad. Stab. 94, 591–596. https://doi.org/10.1016/j.polymdegradstab.2009.01.013

Royer, S.J., Ferrón, S., Wilson, S.T., Karl, D.M., 2018. Production of methane and ethylene from plastic in the environment. PLoS One 13 (8), e0200574. https://doi.org/10.1371/journal.pone.0200574

Rujnić-Sokele, M., Pilipović, A., 2017. Challenges and opportunities of biodegradable plastics: A mini review. Waste Manag. Res. 35, 132–140. https://doi.org/10.1177/0734242X16683272

Schmidt, C., Krauth, T., Wagner, S., 2017. Export of Plastic Debris by Rivers into the Sea. Environ. Sci. Technol. 51, 12246–12253. https://doi.org/10.1021/acs.est.7b02368

Schwarzenbach, R. P., Gschwend, P. M., Imboden, D. M., 2005. Direct Photolysis. In: Environmental organic chemistry, 2nd ed. Wiley, Hoboken, pp. 611–620. https://doi.org/10.1002/0471649643.ch15

Setälä, O., Fleming-Lehtinen, V., Lehtiniemi, M., 2014. Ingestion and transfer of microplastics in the planktonic food web. Environ. Pollut. 185, 77–83. https://doi.org/10.1016/j.envpol.2013.10.013

Setälä, O., Magnusson, K., Lehtiniemi, M., Norén, F., 2016. Distribution and abundance of surface water microlitter in the Baltic Sea: A comparison of two sampling methods. Mar. Pollut. Bull. 110, 177–183. https://doi.org/10.1016/j.marpolbul.2016.06.065

Shah, A.A., Hasan, F., Hameed, A., Ahmed, S., 2008. Biological degradation of plastics: A comprehensive review. Biotechnol. Adv. 26, 246–265. https://doi.org/10.1016/j.biotechadv.2007.12.005

Shank, G.C., Evans, A., Yamashita, Y., Jaffé, R., 2011. Solar radiation - Enhanced dissolution of particulate organic matter from coastal marine sediments. Limnol. Oceanogr. 56, 577–588. https://doi.org/10.4319/lo.2011.56.2.0577

Shao, T., Song, K., Du, J., Zhao, Y., Ding, Z., Guan, Y., Liu, L., Zhang, B., 2016. Seasonal Variations of CDOM Optical Properties in Rivers Across the Liaohe Delta. Wetlands 36, 181–192. https://doi.org/10.1007/s13157-014-0622-2

Sharma, S., Chatterjee, S., 2017. Microplastic pollution, a threat to marine ecosystem and human health: a short review. Environ. Sci. Pollut. Res. 24, 21530–21547. https://doi.org/10.1007/s11356-017-9910-8

Sikorski, R.J., Zika, R.G., 1993a. Modeling mixed-layer photochemistry of H_2O_2: Optical and chemical modeling of production. J. Geophys. Res.: Oceans. 98, 2315–2328. https://doi.org/10.1029/92JC02933

Sikorski, R.J., Zika, R.G., 1993b. Modeling mixed-layer photochemistry of H_2O_2: Physical and chemical modeling of distribution. J. Geophys. Res.: Oceans. 98, 2329–2340. https://doi.org/10.1029/92JC02940

Song, G., Li, Y., Hu, S., Li, G., Zhao, R., Sun, X., Xie, H., 2017. Photobleaching of chromophoric dissolved organic matter (CDOM) in the Yangtze River estuary kinetics and effects of temperature, pH, and salinity. Environ. Sci. Process. Impacts 19, 861–873. https://doi.org/10.1039/c6em00682e

Song, G., Xie, H., 2017. Spectral efficiencies of carbon monoxide photoproduction from particulate and dissolved organic matter in laboratory cultures of Arctic sea ice algae. Mar. Chem. 190, 51–65. https://doi.org/10.1016/j.marchem.2017.02.002

Song, G., Xie, H., Bélanger, S., Leymarie, E., Babin, M., 2013. Spectrally resolved efficiencies of carbon monoxide (CO) photoproduction in the western Canadian Arctic: Particles versus solutes. Biogeosciences 10, 3731–3748. https://doi.org/10.5194/bg-10-3731-2013

Song, Y.K., Hong, S.H., Jang, M., Kang, J.H., Kwon, O.Y., Han, G.M., Shim, W.J., 2014. Large accumulation of micro-sized synthetic polymer particles in the sea surface microlayer. Environ. Sci. Technol. 48, 9014–9021. https://doi.org/10.1021/es501757s

Stein, R., Macdonald, R.W., 2004. Organic carbon budget: Arctic Ocean vs. global ocean. In: The organic carbon cycle in the Arctic Ocean. Springer, Berlin, Heidelberg, pp. 315–322. https://doi.org/10.1007/978-3-642-18912-8_8

Sussarellu, R., Suquet, M., Thomas, Y., Lambert, C., Fabioux, C., Pernet, M.E.J., Goïc, N. Le, Quillien, V., Mingant, C., Epelboin, Y., Corporeau, C., Guyomarch, J., Robbens, J., Paul-Pont, I., Soudant, P., Huvet, A., 2016. Oyster reproduction is affected by exposure to polystyrene microplastics. Proc. Natl. Acad. Sci. U. S. A. 113, 2430–2435. https://doi.org/10.1073/pnas.1519019113

Talsness, C.E., Andrade, A.J.M., Kuriyama, S.N., Taylor, J.A., Saal, F.S.V., 2009. Components of plastic: Experimental studies in animals and relevance for human health. Philos. Trans. R. Soc. B Biol. Sci. 364, 2079–2096. https://doi.org/10.1098/rstb.2008.0281

Tang, C.C., Chen, H.I., Brimblecombe, P., Lee, C.L., 2019. Morphology and chemical properties of polypropylene pellets degraded in simulated terrestrial and marine environments. Mar. Pollut. Bull. 149, 110626. https://doi.org/10.1016/j.marpolbul.2019.110626

Thompson, R.C., Olsen, Y., Mitchell, R.P., Davis, A., Rowland, J., John, A.W.G., Mcgonigle, D., Russell, A.E., 2004. Lost at Sea : Where Is All the Plastic ? Published by : American Association for the Advancement of Science Stable URL : http://www.jstor.com/stable/3836916 304, 4–5.

Tian, L., Chen, Q., Jiang, W., Wang, L., Xie, H., Kalogerakis, N., Ma, Y., Ji, R., 2019. A carbon-14 radiotracer-based study on the phototransformation of polystyrene nanoplastics in water: Versus in air. Environ. Sci. Nano 6, 2907–2917. https://doi.org/10.1039/c9en00662a

Tidjani, A., 1997. Photooxidation of polypropylene under natural and accelerated weathering conditions. J. Appl. Polym. Sci. 64, 2497–2503. https://doi.org/10.1002/(SICI)1097-4628(19970627)64:13<2497::AID-APP3>3.0.CO;2-8

Toole, D.A., Kieber, D.J., Kiene, R.P., Siegel, D.A., Nelson, N.B., 2003. Photolysis and the dimethylsulfide (DMS) summer paradox in the Sargasso Sea. Limnol. Oceanogr. 48, 1088–1100. https://doi.org/10.4319/lo.2003.48.3.1088

Tsang, Y.Y., Mak, C.W., Liebich, C., Lam, S.W., Sze, E.T.P., Chan, K.M., 2017. Microplastic pollution in the marine waters and sediments of Hong Kong. Mar. Pollut. Bull. 115, 20–28. https://doi.org/10.1016/j.marpolbul.2016.11.003

Turner, A. and Holmes, L.A., 2015. Adsorption of trace metals by microplastic pellets in fresh water. Environ. Chem. 12, 600–610. https://doi.org/10.1071/EN14143

Van Cauwenberghe, L., 2016. Occurrence, effects and risks of marine microplastics. Thesis Submitted in Fulfilment of the Requirements for the Degree of Doctor (PhD) in Applied Biological Sciences. Ghent University, Belgium, pp. 16–18.

Van Cauwenberghe, L., Janssen, C.R., 2014. Microplastics in bivalves cultured for human consumption. Environ. Pollut. 193, 65–70. https://doi.org/10.1016/j.envpol.2014.06.010

van der Hal, N., Ariel, A., Angel, D.L., 2017. Exceptionally high abundances of microplastics in the oligotrophic Israeli Mediterranean coastal waters. Mar. Pollut. Bull. 116, 151–155. https://doi.org/10.1016/j.marpolbul.2016.12.052

Von Hobe, M., Najjar, R.G., Kettle, A.J., Andreae, M.O., 2003. Photochemical and physical modeling of carbonyl sulfide in the ocean. J. Geophys. Res.: Oceans. 108, 3229. https://doi.org/10.1029/2000JC000712

Ward, C.P., Armstrong, C.J., Walsh, A.N., Jackson, J.H., Reddy, C.M., 2019. Sunlight Converts Polystyrene to Carbon Dioxide and Dissolved Organic Carbon. Environ. Sci. Technol. Lett. 6, 669–674. https://doi.org/10.1021/acs.estlett.9b00532

Watts, A.J.R., Lewis, C., Goodhead, R.M., Beckett, S.J., Moger, J., Tyler, C.R., Galloway, T.S., 2014. Uptake and retention of microplastics by the shore crab carcinus maenas. Environ. Sci. Technol. 48, 8823–8830. https://doi.org/10.1021/es501090e

Weishaar, J.L., Aiken, G.R., Bergamaschi, B.A., Fram, M.S., Fujii, R., Mopper, K., 2003. Evaluation of specific ultraviolet absorbance as an indicator of the chemical composition and reactivity of dissolved organic carbon. Environ. Sci. Technol. 37, 4702–4708. https://doi.org/10.1021/es030360x

Wright, S.L., Rowe, D., Thompson, R.C., Galloway, T.S., 2013a. Microplastic ingestion decreases energy reserves in marine worms. Curr. Biol. 23, R1031–R1033. https://doi.org/10.1016/j.cub.2013.10.068

Wright, S.L., Thompson, R.C., Galloway, T.S., 2013b. The physical impacts of microplastics on marine organisms: a review. Environ. Pollut. 178, 483–492. https://doi.org/10.1016/j.envpol.2013.02.031

Wu, X., Liu, P., Shi, H., Wang, H., Huang, H., Shi, Y., Gao, S., 2021. Photo aging and fragmentation of polypropylene food packaging materials in artificial seawater. Water Res. 188, 116456. https://doi.org/10.1016/j.watres.2020.116456

Xie, H., Bélanger, S., Song, G., Benner, R., Taalba, A., Blais, M., Tremblay, J.E., Babin, M., 2012. Photoproduction of ammonium in the southeastern Beaufort Sea and its biogeochemical implications. Biogeosciences 9, 3047–3061. https://doi.org/10.5194/bg-9-3047-2012

Xie, H., Zafiriou, O.C., 2009. Evidence for significant photochemical production of carbon monoxide by particles in coastal and oligotrophic marine waters. Geophys. Res. Lett. 36, 1–5. https://doi.org/10.1029/2009GL041158

Yang, D., Shi, H., Li, L., Li, J., Jabeen, K., Kolandhasamy, P., 2015. Microplastic Pollution in Table Salts from China. Environ. Sci. Technol. 49, 13622–13627. https://doi.org/10.1021/acs.est.5b03163

Yocis, B.H., Kieber, D.J., Mopper, K., 2000. Photochemical production of hydrogen peroxide in Antarctic waters. Deep. Res. Part I Oceanogr. Res. Pap. 47, 1077–1099. https://doi.org/10.1016/S0967-0637(99)00095-3

Yousif, E., Haddad, R., 2013. Photodegradation and photostabilization of polymers, especially polystyrene: Review. Springerplus 2, 1–32. https://doi.org/10.1186/2193-1801-2-398

Yujing, M., Mellouki, A., 2000. The near-UV absorption cross sections for several ketones. J. Photochem. Photobiol. A Chem. 134, 31–36. https://doi.org/10.1016/S1010-6030(00)00243-4

Zafiriou, O.C., 2002. Sunburnt organic matter: Biogeochemistry of light-altered substrates. Limnol. Oceanogr. Bull. 11, 69–74. https://doi.org/10.1002/lob.200211469

Zafiriou, O.C., Andrews, S.S., Wang, W., 2003. Concordant estimates of oceanic carbon monoxide source and sink processes in the Pacific yield a balanced global “blue-water” CO budget. Global Biogeochem. Cycles 17. https://doi.org/10.1029/2001GB001638

Zafiriou, O.C., Joussot-Dubien, J., Zepp, R.G., Zika, R.G., 1984. Photochemistry of natural waters. Environ. Sci. Technol. 18, 358A–371A. https://doi.org/10.1021/es00130a001

Zafiriou, O.C., True, M.B., 1979a. Nitrate photolysis in seawater by sunlight. Mar. Chem. 8, 33–42. https://doi.org/10.1016/0304-4203(79)90030-6

Zafiriou, O.C., True, M.B., 1979b. Nitrite photolysis in seawater by sunlight. Mar. Chem. 8, 9–32. https://doi.org/10.1016/0304-4203(79)90029-X

Zepp, R.G., Cline, D.M., 1977. Rates of direct photolysis in aquatic environment. Environ. Sci. Technol. 11, 359–366. https://doi.org/10.1021/es60127a013

Zhang, W., Ma, X., Zhang, Z., Wang, Y., Wang, Juying, Wang, Jing, Ma, D., 2015. Persistent organic pollutants carried on plastic resin pellets from two beaches in China. Mar. Pollut. Bull. 99, 28–34. https://doi.org/10.1016/j.marpolbul.2015.08.002

Zhang, W., Zhang, S., Wang, J., Wang, Y., Mu, J., Wang, P., Lin, X., Ma, D., 2017. Microplastic pollution in the surface waters of the Bohai Sea, China. Environ. Pollut. 231, 541–548. https://doi.org/10.1016/j.envpol.2017.08.058

Zhang, Y., Xie, H., Chen, G., 2006. Factors affecting the efficiency of carbon monoxide photoproduction in the St. Lawrence estuarine system (Canada). Environ. Sci. Technol. 40, 7771–7777. https://doi.org/10.1021/es0615268

Zhang, Z., Hu, X., Luo, Z., 1996. Wavelength sensitivity of photooxidation of polypropylene. Polym. Degrad. Stabil. 51, 93–97. https://doi.org/10.1177/096739111502300205

Zhao, S., Zhu, L., Li, D., 2015. Microplastic in three urban estuaries, China. Environ. Pollut. 206, 597–604. https://doi.org/10.1016/j.envpol.2015.08.027

Zhao, S., Zhu, L., Wang, T., Li, D., 2014. Suspended microplastics in the surface water of the Yangtze Estuary System, China: First observations on occurrence, distribution. Mar. Pollut. Bull. 86, 562–568. https://doi.org/10.1016/j.marpolbul.2014.06.032

Zhu, L., Bai, H., Chen, B., Sun, X., Qu, K., Xia, B., 2018. Microplastic pollution in North Yellow Sea, China: Observations on occurrence, distribution and identification. Sci. Total Environ. 636, 20–29. https://doi.org/10.1016/j.scitotenv.2018.04.182

Zhu, L., Zhao, S., Bittar, T.B., Stubbins, A., Li, D., 2020. Photochemical dissolution of buoyant microplastics to dissolved organic carbon: Rates and microbial impacts. J. Hazard. Mater. 383, 121065. https://doi.org/10.1016/j.jhazmat.2019.121065

Zhu, X., Miller, W.L., Fichot, C.G., 2020. Simple Method to Determine the Apparent Quantum Yield Matrix of CDOM Photobleaching in Natural Waters. Environ. Sci. Technol. 54, 14096–14106. https://doi.org/10.1021/acs.est.0c03605

Zika, R. G., 1981. Marine organic photochemistry. In: Duursma, E.K., Dawson, R. (Eds.), Elsevier Oceanography Series. Elsevier, 31, pp. 299–325. https://doi.org/10.1016/S0422-9894(08)70332-5

SUPPLEMENTARY MATERIALS

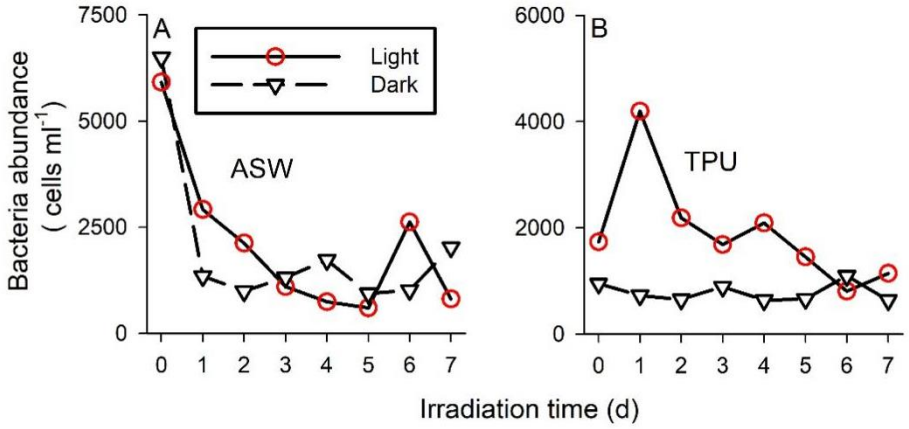

Figure S1. Bacterial cell abundance versus time during irradiation of artificial seawater-only (A) and TPU (B) at 20 ℃.

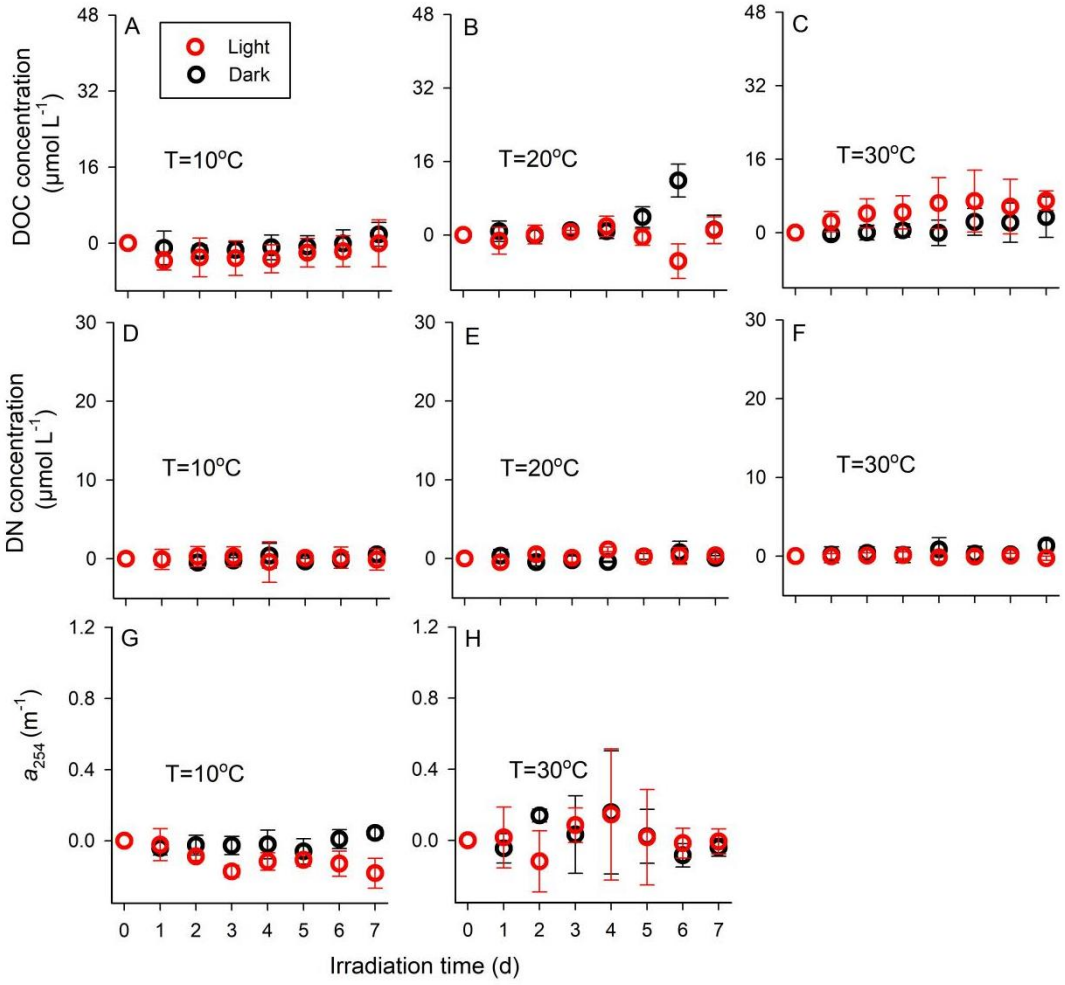

Figure S2. [DOC] (top), [DN] (middle), and a_{254} (bottom) versus time during irradiation of artificial seawater without addition of MPs at different temperatures. Data for dark controls are shown as the measured value at each sampling point minus the time-zero value, while data for light treatments represent the measured value at each sampling point minus the corresponding dark control value.

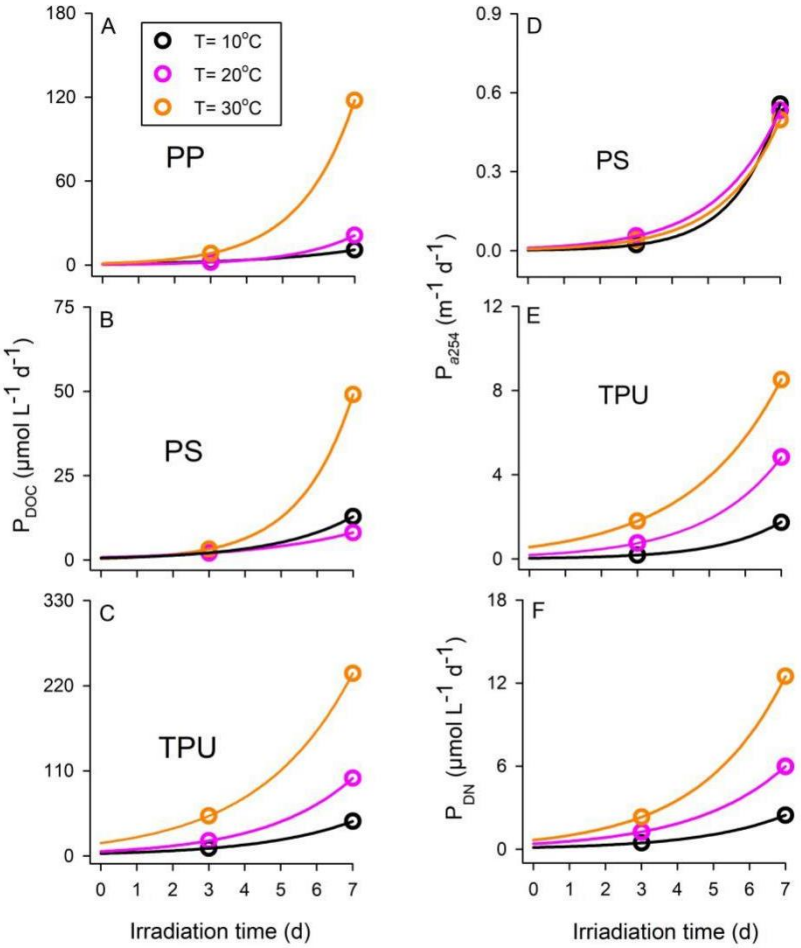

Figure S3. Photorelease rates of DOC, DN, and CDOM (represented by a_{254}) from the tested microplastics irradiated at different temperatures. A-C: P_{DOC}; D and E: P_{CDOM}; F: P_{DN}.

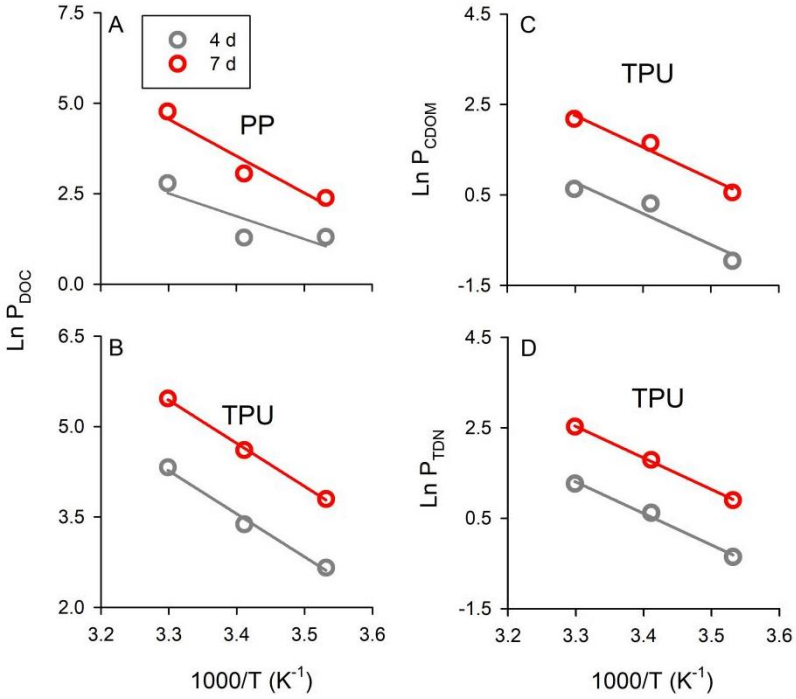

Figure S4. Arrhenius plots of the photorelease rate of DOC (P_{DOC}) (A, B), CDOM (C, represented by a_{254}), and DN (D) at two selected irradiation time points (day 4 and day 7). Lines are best fits of the data. The fitted equations are shown in Table 6 in the main text. PP: polypropylene; TPU: thermoplastic polyurethane.

Table S1: Microplastics abundances in surface seawater worldwide. To facilitate comparison, areal abundance is converted to volumetric abundance (i.e. standardized abundance) using the sampling depth reported. ptc: particles

Location	Measured abundance	Standardized abundance	Sample depth	Mesh size (μm)	Reference
Coastal seas					
Northwest Mediterranean	0.116 ptc m^{-2}	1.16 ptc m^{-3}	<10 cm	330	Collignon et al., 2012
Sardinian Sea, Western Mediterranean	0.15 ptc m^{-3}		<50 cm	500	de Lucia et al., 2014
West coast Vancouver Island	1710 ± 1110 ptc m^{-3}				
Queen Charlotte Sound	7630 ± 1410 ptc m^{-3}		4.5 m	250, 125, 62.5	Desforges et al., 2014
Strait of Georgia	3210 ± 628 ptc m^{-3}				
Yangtze Estuary, China	4137.3 ± 2461.5 ptc m^{-3}		1 m	32	Zhao et al., 2014
East China Sea	0.167 ± 0.138 ptc m^{-3}		<30 cm	333	
Geoje Island, South Korea	16,272 ptc m^{-3}		150–400 μm	0.75	Song et al., 2014
	213 ± 141 ptc m^{-3}			0.75	
	1143 ± 3353 ptc m^{-3}		<20 cm	50	
	47 ± 192 ptc m^{-3}			330	
Urban estuaries, China	680.0–1245.8 ptc m^{-3}		<30 cm	333	Zhao et al., 2015

East Asian seas around Japan	3.74 ± 10.40 ptc m^{-3}		<75 cm	350	Isobe et al., 2015
Incheon/Kyeonggi Coastal Region. South Korea	152 688 ± 92 384 ptc m^{-3}		<400 μm	0.75	Chae et al., 2015
	1602 ± 1274 ptc m^{-3}		<30 cm	20	
	0.19 ± 0.14 ptc m^{-3}			330	
Southeastern coast of Korea	1.92–5.51 ptc m^{-3} (<2 mm) 2.30–38.77 ptc m^{-3} (2–5 mm)		<20 cm	330	Kang et al., 2015
	582–924 ptc m^{-3} (<2 mm) 10–375 ptc m^{-3} (2–5 mm)			50	
Baltic Sea, Gulf of Finland	0–0.8 ptc m^{-3}		<0.25 m	333	Setälä et al., 2016
	0–1.25 ptc m^{-3}		0–0.5 m	300	
	0–6.8 ptc m^{-3}			100	
Victoria Harbour, HongKong, China	27,909 ± 7407 ptc/100 m^3	279.09 ± 74.07 ptc m^{-3}	No detail	153	Tsang et al., 2017
Bohai Sea, China	0.33 ± 0.34 ptc m^{-3}		<45 cm	330	Zhang et al., 2017
Iskenderun Bay, Northeastern Levantine coast of Turkey	1,067,120 ptc km^{-2}	7.11 ptc m^{-3}	<15 cm	333	Gündoğdu, 2017
Israeli Mediterranean coast	7.68 ± 2.38 ptc m^{-3}		<10 cm	333	van der Hal et al., 2017
North Yellow Sea	545 ± 282 ptc m^{-3}		<30 cm	30	Zhu et al., 2018
Southern North Sea	27.2 ± 52.5 ptc m^{-3}		<15 cm	100	Lorenz et al., 2019

Open oceans					
North Pacific Central Gyre	309,506 pieces km^{-2} (micro: 0.355–4.76 mm)	2.06 ptc m^{-3}	<15 cm	333	Moore et al., 2001
North Pacific subtropical gyre	0.021–0.448 ptc m^{-2}, maximum : 6.553 ptc m^{-2}	0.105–2.24 ptc m^{-3}, maximum: 32.76 ptc m^{-3}	<20 cm	330	Goldstein et al., 2013
South Pacific subtropical gyre	24,499 pieces km^{-2} (micro: 0.355–4.75 mm)	0.153 ptc m^{-3}	<16 cm	330	Eriksen et al., 2013
Northeast Pacific Ocean	279 ± 178 ptc m^{-3}		4.5 m	250, 125, 62.5	Desforges et al., 2014
Northwestern Pacific Ocean	0.14 ptc m^{-3}		<45 cm	330	Pan et al., 2019
North Atlantic Gyre	1.69 ptc m^{-3}		<50 cm	150	Reisser et al., 2015
Northeast Atlantic Ocean	2.46 ± 2.43 ptc m^{-3}		3 m	250	Lusher et al., 2014
Arctic polar waters	0.34 ± 0.31 ptc m^{-3}		<16 cm	250	Lusher et al., 2015
	2.68 ± 2.95 ptc m^{-3}		6 m		
Ross Sea (Antarctica)	0.17 ± 0.34 particle m^{-3}		5 m	1	Cincinelli et al., 2017
Northeast Greenland, Arctic	2.4 ± 0.8 ptc m^{-3}		6 m	80	Morgana et al., 2018

Table S2: The scaling factors (i.e. ratios) of UVB (290-300 nm) irradiance of the SUNTEST CPS solar simulator to those of the reference solar spectrum at latitudes of 0-60oN reported by Apell and McNeil (2019). The irradiances of the reference spectra are daily (24 h) irradiances just above the sea surface on the clear-sky days of March 23, June 19, September 24, and December 19 in 2014. The average scaling factor is the ratio of the solar simulator's UVB irradiance to the average daily UVB irradiance of the reference spectra for the four selected days.

	0°	10°N	20°N	30°N	40°N	50°N	60°N
March Equinox	2.7	2.8	3.2	4.0	5.8	9.6	17.8
Summer solstice	3.4	3.0	2.8	2.8	3.0	3.4	4.1
September Equinox	2.9	3.0	3.2	3.9	5.0	7.7	13.3
Winter solstice	3.1	3.9	5.6	9.4	21.5	76.2	710.3
Average	3.0	3.1	3.5	4.1	5.3	7.5	10.6
	0°–20° N		20°–40° N		40°–60° N		
March Equinox	2.9		4.1		9.0		
Summer solstice	3.0		2.9		3.5		
September Equinox	3.0		3.9		7.4		
Winter solstice	4.0		9.0		49.1		
Average	3.2		4.2		7.2		